Computers, Materials & Continua

Tech Science Press

DOI: 10.32604/cmc.2024.054691

REVIEW

First Principles Calculations for Corrosion in Mg-Li-Al Alloys with Focus on Corrosion Resistance: A Comprehensive Review

Muhammad Abdullah Khan[1], Muhammad Usman[2] and Yuhong Zhao[1,3,4,*]

[1]School of Materials Science and Engineering, Collaborative Innovation Center of Ministry of Education and Shanxi Province for High-Performance Al/Mg Alloy Materials, North University of China, Taiyuan, 030051, China

[2]Electronics Department, North University of China, Taiyuan, 030000, China

[3]Beijing Advanced Innovation Center for Materials Genome Engineering, University of Science and Technology Beijing, Beijing, 100083, China

[4]Institute of Materials Intelligent Technology, Liaoning Academy of Materials, Shenyang, 110004, China

*Corresponding Author: Yuhong Zhao. Email: zhaoyuhong@nuc.edu.cn

Received: 05 June 2024 Accepted: 30 September 2024 Published: 18 November 2024

ABSTRACT

This comprehensive review examines the structural, mechanical, electronic, and thermodynamic properties of Mg-Li-Al alloys, focusing on their corrosion resistance and mechanical performance enhancement. Utilizing first-principles calculations based on Density Functional Theory (DFT) and the quasi-harmonic approximation (QHA), the combined properties of the Mg-Li-Al phase are explored, revealing superior incompressibility, shear resistance, and stiffness compared to individual elements. The review highlights the brittleness of the alloy, supported by B/G ratios, Cauchy pressures, and Poisson's ratios. Electronic structure analysis shows metallic behavior with varied covalent bonding characteristics, while Mulliken population analysis emphasizes significant electron transfer within the alloy. This paper also studied thermodynamic properties, including Debye temperature, heat capacity, enthalpy, free energy, and entropy, which are precisely examined, highlighting the Mg-Li-Al phase sensitive to thermal conductivity and thermal performance potential. Phonon density of states (PHDOS) confirms dynamic stability, while anisotropic sound velocities reveal elastic anisotropies. This comprehensive review not only consolidates the current understanding of the Mg-Li-Al alloy's properties but also proposes innovative strategies for enhancing corrosion resistance. Among these strategies is the introduction of a corrosion barrier akin to the Mg-Li-Al network, which holds promise for advancing both the applications and performance of these alloys. This review serves as a crucial foundation for future research aimed at optimizing alloy design and processing methods.

KEYWORDS

First-principles calculations; Mg-Li-Al alloys; corrosion resistance; thermodynamic properties; mechanical properties

1 Introduction

Magnesium alloys are lightweight structural components in transportation industries because of their high specific strength and low density [1–3]. Magnesium alloys are also extensively utilized

in aerospace [4], military, energy, and biological sectors [5,6]. Their density ranges from 1.35 to 1.65 g/cm^3, making them the least dense among current metal materials [7]. However, the corrosion occurring in atmospheric and aqueous environments is a significant obstacle to the broader adoption of magnesium alloys [5,8]. Corrosion of magnesium can be significantly reduced by applying various surface treatments after the forming process. These post-forming treatments enhance the durability and resistance of magnesium against environmental factors that typically cause corrosion [9]. The enhancement of corrosion resistance in magnesium alloys is frequently achieved by adding alloying elements. Mg alloys, characterized by their exceptional light weight, demonstrate notable corrosion resistance in a 0.1 M NaCl solution, particularly when containing substantial amounts of lithium (Li). This improved resistance is due to the formation of a uniform Li_2CO_3 coating on the alloy surface [10,11]. Introducing aluminum (Al) to Mg-Li alloys further augments corrosion resistance by increasing the hydrogen overpotential, thereby inhibiting exfoliation corrosion. This results in a dense $Mg(OH)_2$/Al coating that mitigates further corrosive degradation [12]. Moreover, incorporating rare earth elements in Mg alloys can reduce micro-galvanic corrosion and facilitate the development of protective layers, leading to significantly enhanced corrosion resistance [13,14]. Corrosion of magnesium proceeds for pH levels below 11, as oxygen does not participate in the reaction and no passivating surface layer forms [15,16]. Previous studies have demonstrated that when magnesium [17] is exposed to environments containing chloride, the presence of elements like cobalt (Co), copper (Cu), iron (Fe), and nickel (Ni) can significantly speed up the corrosion process. These elements act as catalysts, making the magnesium more susceptible to deterioration in chloride-rich conditions [18,19].

Galvanic corrosion may occur in a water-based environment when magnesium anodic dissolution regions are connected to the cathodic reduction of water. Pits form in areas of secondary-phase particles, which function as cathodic sites. Magnesium depletion occurs due to this phenomenon [20–22]. Magnesium showed a negative standard electrode potential of −2.37 V compared to the standard hydrogen electrode [23]. This indicates its high reactivity as an anode [24].

The anodic dissolution of Mg:

$$Mg \rightarrow Mg^{2+}2^{e-} \tag{1}$$

The cathodic reduction of water:

$$2H_2O + 2^{e-} \rightarrow H_2(g) + 2OH^- \tag{2}$$

First-principles calculations through DFT have been crucial in exploring cathodic reactions occurring on magnesium and its surfaces of alloys. Velikokhatnyi et al. [25] started DFT-based investigations to examine the thermodynamics reactions between Mg alloys containing trace alloy elements with pure water. DFT calculations employed to examine cathodic reactions on the Mg (0001) surface and later utilized the findings to construct the magnesium Pourbaix diagram [26,27]. Another study by [28] and [29] utilized DFT calculations to analyze cathodic reactions on Mg surfaces doped with various elements. Their findings revealed that specific alloying elements, such as aluminum (Al) and lithium (Li), exhibit the potential to enhance corrosion resistance by mitigating steps in cathode reactions. Similarly, authors [30] used DFT calculation to study the $Mg_{17}Al_{12}$ precipitates in Mg-Al alloys, which serve as cathodic reaction sites [31].

Cathodic reactions on the Mg (0001) surface [26,27]:

$$H_2O + e^- \rightarrow OH^- + \frac{1}{2}H_2 \tag{3}$$

Mg surfaces cathodic reactions doped with Al or Li:

When Al is present:

$$Al^{3+}3e^{-} \rightarrow Al \tag{4}$$

When Li is present:

$$Li^{+} + e^{-} \rightarrow Li \tag{5}$$

Cathodic reaction sites in Mg-Al alloys involving $Mg_{17}Al_{12}$ [31]:

$$Mg_{17}Al_{12} + H_2O \rightarrow Mg(OH)_2 + Al(OH)_3 + H_2 \tag{6}$$

The presence of Al and Li influences the overall corrosion resistance by participating in the reduction reactions and possibly forming protective layers that inhibit further corrosion. The combined effect of these reactions contributes to the alloy's enhanced corrosion resistance by reducing specific steps in the cathodic reaction pathways. Mg corrosion studies involve DFT calculations investigating element binding on cathode sites, particularly on second-phase particles of transition-metal, and their effects on the hydrogen evolution reaction.

Magnesium-lithium (Mg-Li) alloys are highly regarded for their excellent specific mechanical properties, including high stiffness and low density, making them suitable for commercial applications. Magnesium-lithium (Mg-Li) alloys, known for their high stiffness and low density, are ideal for aerospace and automotive industries, where lightweight materials enhance fuel efficiency. They are also used in portable electronics, sporting goods, and military equipment, providing durability and performance without adding significant weight [32,33]. A new ternary alloy, Mg-Li-Al, is formed, which exhibits enhanced hardness and electrical conductivity by incorporating an appropriate amount of magnesium [17] into the binary Mg-Li system [12,34]. The Mg-Li-Al ternary alloys have gained significant research interest due to their promising properties [12,35]. Rahulan et al. [36] reported notable improvements in tensile properties and hardness by adding aluminum to the Mg-Li alloy. Mazlan et al. [37] assessed the ternary Mg-Li-Al phase diagram and its binary sub-systems. Li et al. [38] evaluated various compositions of the Mg-Li-Al alloy, examining tensile strength, properties, and corrosion resistance. He et al. [39] analyzed the oxidation behaviour of Mg-Al-Li alloys with different compositions using thermogravimetric/differential thermal analysis. These studies reflect the considerable interest of researchers in the Mg-Li-Al alloy system. The surface and thermodynamic properties of the liquid Mg-Li-Al ternary alloy have been investigated at various temperatures (1000, 1073, 1150, and 1250 K) utilizing four distinct theoretical models, as documented in previous studies [40]. These investigations provide significant insights into the physical mechanisms through which the addition of alloying or doping elements onto magnesium matrix surfaces can slow down cathodic reactions. However, two critical areas permit further examination. Firstly, although there is evidence indicating that second-phase particles abundant in transition-metal elements function as efficient cathodic reaction sites under specific conditions and current DFT calculations fail to explain the underlying physical mechanisms that hinder cathodic reactions on the surfaces of these second-phase particles. Secondly, the scope of doped elements explored in existing DFT studies remains restricted, highlighting the need for a more extensive investigation to grasp the potential advantages of different alloying elements comprehensively. This review paper aims to address these gaps by critically evaluating existing research and proposing directions for future studies, thereby enhancing our understanding of how alloying and doping can improve the corrosion resistance of Mg-based

materials. Fig. 1 illustrates the schematic flow diagram, outlining the key processes and relationships central to the study's framework.

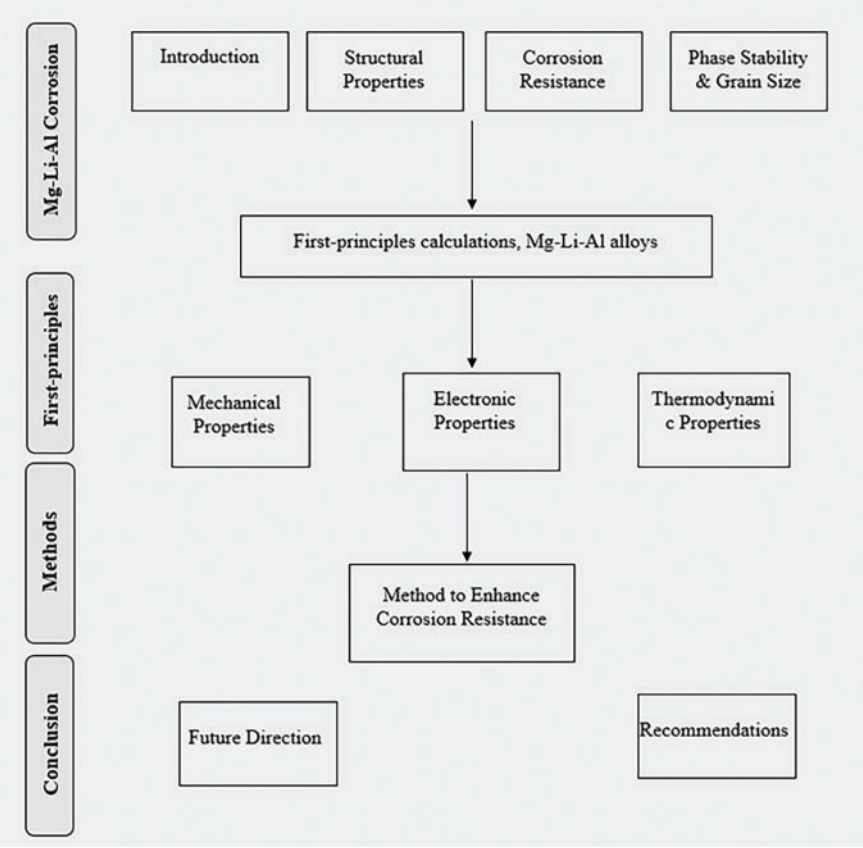

Figure 1: Schematic flow diagram

2 Organizational Structure

2.1 Crystal Structure and Surface Properties of Mg

One of the metals' most important microstructural features, crystallographic orientation, shows how corrosion behaves in a particular environment [41,42]. Different atomic coordination densities within different crystallographic planes cause surface energy levels to fluctuate. Surface energy decreases, anodic dissolution is reduced, and water or proton adsorption is enhanced in densely packed planes due to increased binding energies [43]. For instance, in magnesium, the surface energies of the (1 1 2 0), (1 0 1 0) and (0 0 0 1), planes are recorded as 2.156, 1.868, and 1.808 eV/nm^2, respectively [44], corresponding to 2.99×10^4, 3.04×10^4 and 1.54×10^4 J/mol [45]. Comparatively, the electrochemical degradation rates of alternative crystallographic planes are much greater than those of the base plane (0 0 0 1) [46,47]. Surfaces that are exposed and mostly made of planes with the coordinates (0 0 01) are more resistant to corrosion than those that are mostly made of planes with the coordinates (1 0 1 0) or (1 1 2 0) [43,48]. The formation of oxide coatings in crystalline magnesium alloys is significantly influenced by grain size, as it plays a crucial role in determining the effectiveness of the coating [49]. A study by Ralston et al. [50] showed that the square root of the grain size is inversely associated to the

metals corrosion rate. Magnesium oxide layers can also develop within the surface corrosion layers, enhancing the overall protection against further degradation. By increasing the fraction of volume at grain boundaries, grain refining decreases the lattice mismatch between the oxide layers of crystal structures and the Mg matrix. As a result, this promotes a more cohesive interface, increasing corrosion resistance [51,52]. Also, in passivation, surfaces of refined-grain Mg show faster kinetics, especially in chloride-containing electrolytes. Due to enhanced passivation capacity, the rapid production of magnesium oxide coatings allows these surfaces to withstand breakdowns efficiently [53]. Liu et al. [54] studied grain refining, which showed that it may slow the spread of stress corrosion fractures, especially near grain borders grain size modification is crucial for controlling the corrosion behaviour and durability of Mg alloys. Fig. 2 presents the structural configurations of Mg, Al, and Li, highlighting their atomic arrangements and bonding characteristics.

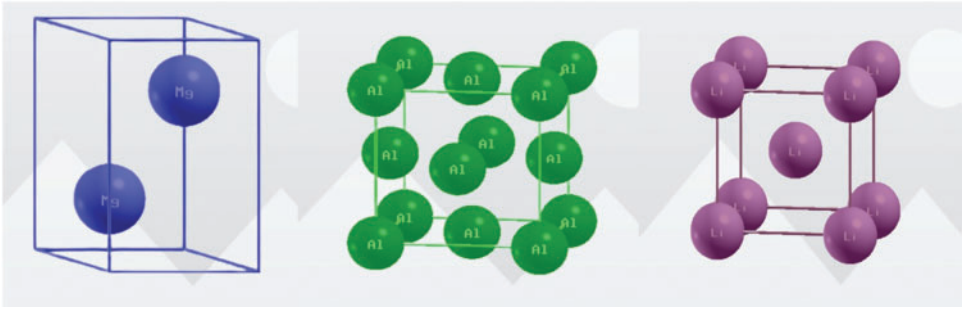

Figure 2: Structure of Mg, Al, and Li

2.2 Instability and Microstructural Development in Mg Alloys

Substantial research was undertaken to understand the mechanisms that enhance the strength and stability of alloying elements in magnesium alloys. Many alloys experience microstructural instability and reduced strength at room temperature over time. However, Mg-Al-Li alloys, known for their relatively stable microstructures, have gained significant attention in the industrial sector. Recent studies by Tang [55] have demonstrated that incorporating aluminum (Al), cadmium (Cd), silver (Ag) and zinc (Zn), into Mg-Li alloys significantly enhances the strengthening effects within the β crystal structure. Tang early research indicated that these ternary alloys could achieve high hardness through water quenching from high temperatures. However, these alloys showed instability below 100°C, leading to microstructural softening. This softening was attributed to the loss of coherency between the θ-phase and the β-matrix due to increased lattice mismatch and the decomposition of the θ-phase into equilibrium phases such as Al-Li and Mg-Li. Reduced strength was linked to coarsening of the θ-phase at grain boundaries, although less so for Li than Al, Zn, and Cd. Recent research by Xin [56] on Mg-Li-Al-based alloys, using modern characterization techniques, has identified a semi-coherent cubic $MgAl_3$ nanophase as the transition phase. It is uncertain if alloys of Li, Ag, Zn, and Cd can adopt this particular structure. The strength at low temperatures is reduced by the decomposition of strengthening precipitates into equilibrium phases such as Mg-Al and Mg-Li, regardless of the transition phase. Based on early studies, several critical observations can be made regarding the stability and strengthening of the β Mg-Li-Al alloys transition phase. Elements with high supersaturated β-phase solubility, such as Al, Li, and Zn, offer the most substantial age-hardening response [57,58]. This occurs because highly soluble elements improve the coherency between the transition phases and the β-matrix, which in turn slows down dislocation motion. Moreover, higher supersaturated solubility typically results in a greater maximum fraction volume of strengthening

precipitates. Conversely, small additions of insoluble elements do not improve the stability and hardening of Mg alloys and provide only limited benefits in Mg alloys [59]. The general elements solubility in the β-solid solution is summarized in Table 1. This knowledge gap suggests an area for potential future research to optimize the mechanical properties of Mg-Li-Al alloys.

Research examined the effects of ternary metals hardening with additions of Ce, La, Nd, and Y in Mg-Li alloys at concentrations of 3–5 wt%. These studies observed a modest increase in strength, approximately 10%–15% higher than that of binary Mg-Li alloys. This increase is notably less than the strengthening achieved with the additions of aluminum (Al), zinc (Zn), silver (Ag), and cadmium (Cd) [60,61]. Although alloys containing rare earth (RE) elements exhibited reduced softening compared to Mg-Li alloys with Zn and Al, the limited strengthening effect rendered RE elements unsuitable as primary alloying agents. Table 1 shows that the alloys failed to harden enough due to eutectic structures formation at the boundaries of grain and the low solubility of the RE components in the solid solution of β-Mg. The strengthening potential of other RE metals with atomic numbers greater than sixty in the β-solid solution remains unexplored [55]. Considering that these elements exhibit high supersaturated solubility in α-Mg [62], it is reasonable that they could also possess high solubility in the β-solid solution, as elements with high solubility in the β phase often exhibit similar behavior in the α phase [57]. Recent research has investigated the alloying of aluminum (Al) or lithium (Li) with magnesium and rare earth (RE) elements [35,39,63]. These studies indicate that such alloying can introduce significant microstructural complexity, including the formation of Mg-AlxREy intermetallic phases. These phases contribute to particle strengthening and may lead to the development of LPSO phases. Chakravorty reported that the Mg11-Li1.5-Al0.14 alloy exhibits stable mechanical properties [64]. Korgiopoulos et al. [65] enhanced the strength of the alloy by increasing the aluminum (Al) content and adding yttrium (Y) to the composition (Mg-10.95, Li-3.29, Al-0.19, Zr-0.59Y). The incorporation of Al_2Y particles refined the microstructure, leading to improved combinations of strength and ductility [66,67]. Additionally, introducing neodymium (Nd) into Mg-Li-Al alloys has enhanced mechanical properties and grain refinement [68]. Conversely, the addition of cerium (Ce) [69] and lanthanum (La) [70] resulted in minimal strengthening effects. LPSO phases have been successfully formed in Mg (α + β)-Al-Li alloys, positively influencing strength and ductility [71]. Table 1 provides the solubility of various elements in magnesium (Mg), highlighting the extent to which each element dissolves within the magnesium matrix.

Table 1: Elements solubility in Mg

Element	Terminal solubility in β Mg	Corrosion resistance contribution	Primary corrosion product	Solubility limit	References
Li	Large	Improves corrosion resistance by forming a protective Li_2CO_3 film	Li_2CO_3	4.6 wt% (room temperature)	[72]
Al	Large	Enhances passivation by forming Al_2O_3	Al_2O_3, $Al(OH)_3$	12.7 wt% (eutectic composition)	[55]
Ag	Large	Increases corrosion resistance through noble metal effect	Ag_2O, Ag_2CO_3	1.5 wt%	[55,59]
Hg	Large	Limited use due to toxicity, but can form protective films	HgO, Hg_2Cl_2	0.1 wt%	[73]
Tl	Large	Forms passive layers, less commonly used	Tl_2O_3, TlOH	0.2 wt%	[55,59]

(Continued)

Table 1 (continued)

Element	Terminal solubility in β Mg	Corrosion resistance contribution	Primary corrosion product	Solubility limit	References
Zn	Large	Improves galvanic protection in coatings	ZnO, $Zn(OH)_2$	6.2 wt%	[74,75]
Ca	Some	Improves corrosion resistance by forming $CaCO_3$	$CaCO_3$	0.8 wt%	[75]
Ba	Some (<1 wt%)	Contributes to forming a protective $BaCO_3$ layer	$BaCO_3$	0.06 wt%	[73]
Ce	Some (<1 wt%)	Enhances passivation, rare earth effect	CeO_2	0.6 wt%	[76,77]
Co	Some (<1 wt%)	Forms protective layers, less commonly used	CoO, $Co(OH)_2$	1.2 wt%	[73]
Cu	Some (<1 wt%)	It forms a protective Cu_2O layer but can promote galvanic corrosion	Cu_2O, $Cu(OH)_2$	0.3 wt%	[78]
Ge	Some (<1 wt%)	Limited data forms GeO_2	GeO_2	0.15 wt%	[79]
La	Some (<1 wt%)	Rare earth element enhances corrosion resistance	La_2O_3	0.45 wt%	[60,61]
Nd	Some (<1 wt%)	Improves passivation, rare earth effect	Nd_2O_3	0.35 wt%	[60,61]
Sn	Some (<1 wt%)	Forms SnO_2, enhancing corrosion resistance	SnO_2	0.9 wt%	[80]
Sr	Some (<1 wt%)	Improves passivation, limited use	$SrCO_3$	0.6 wt%	[81,82]
Y	Some (<1 wt%)	Rare earth element enhances passivation	Y_2O_3	0.3 wt%	[60,61]
B	Insoluble (<0.1 wt%)	Limited corrosion data available	B_2O_3	<0.1 wt%	[83]
Cr	Insoluble (<0.1 wt%)	Forms Cr_2O_3, enhancing passivation	Cr_2O_3	<0.1 wt%	[84,85]
Fe	Insoluble (<0.1 wt%)	Promotes galvanic corrosion if not controlled	Fe_2O_3	<0.1 wt%	[86,87]
Mn	Insoluble (<0.1 wt%)	Enhances corrosion resistance by forming MnO_2	MnO_2	<0.1 wt%	[86]
Mo	Insoluble (<0.1 wt%)	Forms MoO_3, improving passivation	MoO_3	<0.1 wt%	[60,61]
Th	Insoluble (<0.1 wt%)	Limited corrosion data, toxic	ThO_2	<0.1 wt%	[88]
Ti	Insoluble (<0.1 wt%)	Forms TiO_2, enhancing passivation	TiO_2	<0.1 wt%	[60,61]

3 Mg-Li-Al Alloys Corrosion Characteristics

Magnesium determines significant chemical reactivity, characterized by a standard electrode potential of −2.37 V, rendering it vulnerable to the formation of oxides and hydroxides through electrochemical and chemical interactions in atmospheric and marine environments. According to the weight-loss method, the basic rate of corrosion of pure magnesium in sodium chloride is around 0.3 mm/a [89]. In comparison, other Mg alloys, such as Mg-Li-Al, generally display higher corrosion rates in NaCl solutions, typically exceeding 1 mm/a. The high reactivity and corrosion rates in Mg-Li-Al alloys are largely due to the presence of lithium (Li), which has a standard potential of −3.04 V. Lithium is even more reactive than Mg, leading to more pronounced corrosion and erosion in Mg-Li alloys [90]. However, some Mg alloys, such as Mg-4Y-3Nd, exhibit significantly lower corrosion rates of around 0.1 mm/a in chloride solutions [91]. Recent studies [92,93] have demonstrated that Mg-Li alloys exhibit corrosion rates ranging from 0.8 mm/a in 0.1 mol/L solutions of NaCl to 10 mm/a in 3.5 wt% solutions of NaCl. While these rates surpass the basic rate of corrosion of pure Mg, they remain lower compared

to many other Mg alloys. The alloying elements in Mg alloys typically have more positive potentials than Mg, which results in the formation of cathodic second phases that enhance galvanic corrosion of the Mg anode. In Mg-Li alloys, the preferential dissolution of Li leaves behind Mg, which then corrodes or detaches, thereby compromising the alloy's corrosion resistance. The addition of aluminum (Al) to Mg-Li alloys introduces complexity. Al, having a more positive potential than Mg and Li, forms additional cathodic sites that may intensify micro-galvanic corrosion. However, Al can also form a protective oxide layer, potentially mitigating some corrosion. Therefore, Al influences the Mg-Li alloys corrosion behavior, which requires careful balancing to optimize overall performance [12,34].

In aqueous environments, Mg undergoes hydrogen evolution at cathode and dissolution at anode, a process mirrored in Mg alloys. Alloying elements such as Li and Al also dissolve at the anode. Given the reactivity of Mg, Li, and Al in water, the corrosion reactions for Mg-Li-Al alloys can be described by the following reactions [94]:

Cathode reaction/cathodic hydrogen evolution (water reduction):

$$2H_2O + 2^{e-} \rightarrow H_2 \uparrow + 2OH^- \tag{7}$$

Anode reaction/anodic dissolution:

$$Mg \rightarrow Mg^{2+}2^{e-} \tag{8}$$

$$Li \rightarrow Li^+ + e^- \tag{9}$$

$$Al \rightarrow Al^{3+} + 3^{e-} \tag{10}$$

Corrosion products formation:

$$Mg^{2+} + 2OH^- \rightarrow Mg(OH)_2 \tag{11}$$

$$Li^+ + OH^- \rightarrow LiOH \tag{12}$$

$$Al^{3+} + 3OH^- \rightarrow Al(OH)_3 \tag{13}$$

Overall reaction:

$$Mg + 2Li + Al + 7H_2O \rightarrow Mg(OH)_2 + 2LiOH + Al(OH)_3 + \frac{2}{7}H_2 \uparrow \tag{14}$$

The anodic reaction encompasses the complete anodic dissolution process, which involves several intermediate stages. These stages include the formation of partially protective surface films, the presence of uni-positive Mg^{2+} ions, the generation of cathodic catalytic activity, Mg hydride, and various mechanisms of corrosion.

When exposed to CO_2 and O_2, the corrosion products will undergo further reactions as follows:

Formations of carbonates when reacting with CO_2:

$$Mg(OH)_2 + CO_2 \rightarrow MgCO_3 + H_2O \tag{15}$$

$$2LiOH + CO_2 \rightarrow Li_2CO_3 \tag{16}$$

$$2Al(OH)_3 + 3CO_2 \rightarrow Al_2(CO_3)_3 + 3H_2O \tag{17}$$

Formations of Oxides when reacting with O_2:

$$2Mg^{2+} + O_2 \rightarrow 2MgO \tag{18}$$

$$4Li^{+} + O_2 \rightarrow 2Li_2O \quad (19)$$

$$4Al + 3O_2 \rightarrow 2Al_2O_3 \quad (20)$$

The subsequent reactions significantly impact the overall corrosion behavior and properties of the corrosion layer in Mg-Li-Al alloys. Variations in lithium (Li) lead to different crystal structures in Mg-Li alloys, and both the Li content and the crystal structure are crucial in determining their corrosion behavior. Moreover, aluminum (Al) as an alloying element further affects the corrosion characteristics of Mg-Li alloys.

Extensive research has been conducted to investigate the effects of Li content, crystal structure, and Al alloying on the corrosion behavior of Mg alloys, with key findings summarized. He et al. [39] have shown Mg-Li-Al alloys corrosion behavior differs from traditional Mg alloys over time, after 24 h of immersion in a 3.5 wt% NaCl solution, the rate of corrosion of Mg-Li-Al alloy was lower than that of pure Mg. While pure Mg initially exhibited superior corrosion resistance, the Mg-Li-Al alloy displayed smaller and shallower corrosion pits on its surface. Similarly, research by Song et al. [43] compared the dual-phase corrosion performance of Mg-8.8Li alloy with traditional alloy of Mg (AZ91D). Initially, the AZ91D alloy exhibited better corrosion resistance than the Mg-8.8Li alloy, as indicated by electrochemical impedance spectroscopy results and polarization curve. However, after 48 h of immersion, the mass loss rate of the Mg-8.8Li alloy decreased and was lower than that of other alloys (AZ91D). This was attributed to the higher Li activity, which causes rapid Mg-8.8Li alloy corrosion at the start of immersion. Al in the AZ91D alloy promotes passivation of surface. However, the AZ91D protective surface film gradually degrades as corrosion progresses, leading to severe corrosion (galvanic) between the cathodic second phase and the Mg matrix with bottom corrosion pits.

In the corrosion mechanisms of Mg-Li alloys, Wang et al. [95] documented the filiform corrosion characteristics in Mg-8Li alloy. This type of corrosion predominantly occurs at the edge between the β-Li phase and the α-Mg phase, progressing into the β phase due to its higher reactivity. Once the acidic Mg at the filament's tip breaks down, the corrosion products—LiOH and $Mg(OH)_2$—passivate the tail in an alkaline environment, marking the beginning of corrosion. The presence of lithium accelerates hydrogen generation at the cathode, thereby expediting the propagation of filaments. Recent research has indicated that corrosion within the α-Mg phase typically adopts a filiform pattern following initial damage near the phase contact, while intergranular corrosion tends to manifest within the β-Li phase [96]. Feng et al. [97] asserted that the corrosion resistance of Mg-Li alloys is enhanced by accumulating a protective layer composed of thick Li_2CO_3 on their surface. This enhancement is attributed to the low standard enthalpy and high chemical stability of Li_2CO_3, which has a PBR value of approximately 1.27. The formation of a passivated Li_2CO_3 layer on Mg and Mg-Li alloys is facilitated by a homogeneous nanoscale microstructure in Mg-Li-Al-Y-Zr alloys. Recently, Yan et al. [98] utilized various analytical techniques (*in-situ*) to determine the Mg-Li alloy stability in water. This stability is attributed to Li-doped MgO film formation, Li-Al layered double hydroxide (LDH), and a Mg-Li phase of Li-lean hcp beneath the oxide film. Researchers should employ conventional methods to determine the rate of corrosion and parameters associated with Mg-Li-Al alloys and clarify the relationship between microstructure and corrosion behavior. These include gravimetric techniques, optical and electron microscopy, visual inspection, electrochemical measurements and hydrogen gas collection [99,100]. These methodologies provide critical insights into the corrosion mechanisms and offer a comprehensive understanding of the alloy's performance under various environmental conditions. Fig. 3 demonstrates the correlation between the corrosion rate and the intensity of crystallographic planes in an AZ31 magnesium alloy when exposed to 3.5 wt% NaCl solution.

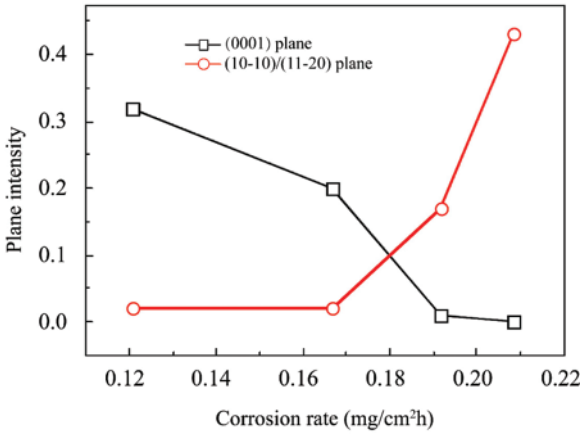

Figure 3: Correlation between the corrosion rate and intensity of crystallographic planes in an AZ31 magnesium alloy exposed to 3.5 wt% NaCl. Reprinted/adapted with permission from Reference [45]. Copyright 2011, Elsevier

4 Methods of Improving Corrosion Behaviour of Mg-Li-Al Alloys

4.1 Alloying

Alloying represents a widespread method employed to modify the corrosion characteristics of Mg-Li-Al alloys. The inclusion of alloying elements influences the structure and composition of the surface oxide layer formed during corrosion. This is crucial because the hydroxide or oxide generated on the magnesium surface lacks the same passivation capabilities as aluminum oxides. The addition of elements such as Li, Al, rare earth metals, and others is expected to strengthen the stability and homogeneity of the surface layer composed of oxides like Al_2O_3, Li_2O, and Y_2O_3 [101]. Such expansion establishes a sustainable, stable, and restorable protective function. Nevertheless, the incorporation of alloying elements induces changes in the alloy microstructure, primarily affecting its corrosion kinetics. The extent of solid solubility of alloying elements in magnesium dictates whether they will precipitate as intermetallic compound phases, magnesium-based solid solutions, or impurity particles. These variables significantly influence the corrosion behavior of magnesium alloys [88].

Aluminum, zinc, and calcium serve as alloying elements in magnesium-lithium alloys. Incorporating aluminum into magnesium-lithium alloys enhances both the hydrogen and the composition and structure of the oxide coating. In biological environments, the rate of degradation of the LAZ631 alloy, characterized by a high aluminum (Al) content, is observed to be slower than the LAZ611 alloy. This disparity can be primarily attributed to the higher Al concentration in the LAZ631 alloy, resulting in a more stable surface layer that facilitates the passivation process. Furthermore, the addition of aluminum (Al) induces a transformation of dendritic crystals into equiaxial crystals, consequently reducing grain size noticeably [35]. With an increase in Al content, additional phases such as $Mg_{17}Al_{12}$ and Mg-Li phases are formed, creating micro-galvanic couplings within the matrix, thereby accelerating corrosion. The proportion of the Al-Li phase increases when introducing varying amounts of aluminum (Al) into a magnesium-lithium (Mg-14Li) alloy, forming a network at the grain boundaries. Consequently, the corrosion rate initially decreases, eventually increasing [39]. In NaCl solution of 0.7 mol/L, Kumar et al. [102] observed that the Mg-8Li-3Al-1Zn electrode demonstrates a higher corrosion potential and a lower corrosion current density than the Mg-8Li-3Al-0.5Zn electrode. This observation is attributed to the formation of uniform and fine products on the electrode's surface.

The introduction of calcium (Ca) into magnesium-lithium alloys, such as Mg-4Li [103], Mg-7Li-3Al [104], and Mg-14Li [105], results in a enhances corrosion resistance and reduction in grain size.

4.2 Impurity Elements

The effect of impurity elements on Mg-Li-Al corrosion resistance differs noticeably from observed traditional Mg alloys. Even a minute quantity of iron in Mg alloys can substantially reduce their resistance to corrosion. A particular concentration threshold exists beyond which the corrosion rate accelerates sharply once the iron content surpasses 0.016%. However, in Mg-Li-Al alloys, the rate of corrosion shows a linear increase with rising Fe concentration, devoid of any distinct threshold [106]. Moreover, the corrosion rate of Mg-Li-Al alloys containing minimal levels of Fe is not significantly higher than that of commercial Mg alloys with hcp-structured [107].

4.3 Rare Elements

Incorporating rare earth (RE) elements into magnesium alloys yield several improvements, including refining the molten metal, enhancing grain structure, reducing potential differences between main and secondary phases, and altering the surface layers structure and composition. The standard electrode potential against SCE remains consistent at −2.372 V for both yttrium (Y) and magnesium. Coating the alloy's surface with a thick layer of yttrium oxide (Y_2O_3) further enhances its corrosion resistance [108]. When yttrium (Y) is introduced into Mg-8Li-3Al-2Zn alloy, the quantity of AlLi phase decreases, transforming the α-Mg shape from elongated needles to more rounded forms [109]. The formation of an Al_2Y phase at grain boundaries prevents galvanic corrosion, unlike the α-Mg and β-Li phases. A reduction in AlLi content within the phase reduces corrosion within the Ξ-Li phase. For instance, in the LAZ832-1.5Y alloy, corrosion current densities of 83.757×10^{-6} A/cm^2 and 21.065×10^{-6} A/cm^2 illustrate a significant decrease in corrosion rate upon yttrium (Y) addition [109]. The formation of Al_2O_3 and Y_2O_3, facilitated by the migration of Y and Al atoms within the Al_2Y/LA143 composite, reduces long-term corrosion rates by impeding the ingress of Cl^- ions into the matrix [110]. Similarly, tin and yttrium (Y) in Mg-5Li-3Al-2Zn alloy reduce grain size, impede the formation of the AlLi phase, resulting in shorter corrosion pits and cracks, and lower corrosion current densities of 9.304×10^{-5} A/cm^2 [111]. Moreover, the presence of cerium (Ce), neodymium (Nd), and gadolinium (Gd) promotes the Al_2(Ce, Nd, Gd) formation with a secondary phase in Mg-Li-Al alloys. RE elements also influence the discharge and corrosion performance of Mg-Li alloys when utilized for batteries. Yttrium and lanthanum additions enhance the alloy's corrosion resistance and electrochemical activity, improving battery performance [112,113].

4.4 Deformation

Mechanical operations such as rolling, extrusion, and severe plastic deformation can significantly alter the microstructure of Mg-Li-Al alloy, impacting its behavior under corrosion conditions. These processes lead to changes in various microstructure properties of Mg alloys, including grain size, presence of secondary phases, dislocation density, and couple creation, which can drastically affect the corrosion rates exhibited by different Mg alloys. In their study, Cao et al. [114] studied the characteristics of corrosion of hot-rolled Mg-X alloys, where X represents elements such as Ca, Gd, Al, Sn, Mn, Sr, La, Nd, Ce, Si or Zr. They found that after hot rolling, the rate of corrosion decreased for most Mg-X alloys, attributed to the formation of more sophisticated secondary phases with a more uniform distribution. However, the corrosion rate increased for Mg-0.1Zr and Mg-0.3Si alloys due to forming an iron-rich phase on the rolled surface. Similarly, after equal channel extrusion, the

corrosion rate of the AZ31 alloy significantly increased, mainly due to the increased dislocation and twin densities within the alloy microstructure [100].

Plastic deformation induces recrystallization, characterized by the development of small grains and redistribution of the second phase, which enhances corrosion resistance by creating a more microstructure (homogeneous). Dynamic recrystallization reduces the grain size of Mg-4Li-Al alloy from 100 to 5 μm during hot rolling [115]. The improved corrosion resistance observed in Mg-9Li-3Al-1.6Y alloy [116] and as-extruded Mg-11Li-3Al-2Zn-1.5Nd-0.2Zr alloy [117] is attributed to the decrease in grain size and consistent intermetallic phases distribution. The grain refinement during deformation in Mg-Li-Al alloys promotes the formation of crystal nuclei, which inhibit the formation of larger grains, thereby reducing dislocation density and energy storage in the material. Microstructural alterations resulting from mechanical deformation influence corrosion behavior. For instance, hot-rolled Mg-Li-Al alloy exhibits pronounced basal roughness parallel to the rolling surface, correlated with a decreased corrosion rate [118]. Ma et al. [119] observed that a 5% reduction in rolling results in more grains oriented perpendicular to the rolling surface, enhancing corrosion resistance. Conversely, a 10% reduction achieves similar results, while a 15% to 20% reduction leads to increased production of extension twins (10/12), promoting the formation of a surface oxide coating that enhances corrosion resistance.

Cross-cold rolling of Mg-Li-Al alloys significantly reduces corrosion rates by forming a uniform and thick layer of corrosion products on the surface [120]. However, plastic deformation, which introduces numerous dislocations and stresses, makes Mg-Li-Al alloys more susceptible to exfoliation corrosion. Exfoliation or pitting corrosion occurs when the oxide layer ruptures in a corrosive environment, leading to delamination along grain boundaries and the formation of tiny fissures. Equiaxed grains may delay fracture initiation, while increased rolling reduction intensifies exfoliation corrosion [121]. Annealing can help mitigate exfoliation corrosion by converting irregularly shaped granules into uniformly sized ones. Wei et al. [122] demonstrated that exfoliation corrosion in extruded Mg-1Li-1Ca alloy results from a combination of intergranular corrosion, filamentous corrosion, pitting corrosion, and stress corrosion, extending from Mg_2Ca particles along grain boundaries. Additionally, the direction of extrusion or rolling ratio affects the extent of exfoliation corrosion, with higher rolling ratios leading to decreased corrosion resistance due to increased microcouplings and area fraction of the β-Li phase [123].

4.5 Heat Treatment

Heat treatment procedures can significantly influence the rate of corrosion. Heat treatment often leads to changes in stress levels, increased atom mobility within the alloy, and the facilitated precipitation or dissolution of subsequent phases. In the case of magnesium alloys, heat treatment plays a crucial role as it alters the quantity and arrangement of secondary phases, thereby affecting corrosion rates [124]. Solution treatment can help establish a continuous corrosion barrier or dissolve secondary phase to delay corrosion. However, heat treatment can also accelerate the formation of iron-rich cathodic phases, potentially leading to faster corrosion rates [11]. In a study by Wang et al. [125], it was found that the β-$(Mg, Zn)_3Gd$ eutectic phase in a Mg-15Gd-2Zn-0.39 Zr alloy resulted from a solid-solution, age-induced transition. This modification reduced micro-galvanic corrosion between the matrix and secondary phase, with the volume fraction and local potential of the LPSO phase significantly smaller than those in the eutectic phase. Various post-deformation processes, including solution treatment, aging, and annealing, can alter the corrosion behavior of Mg-Li-Al alloys. For instance, after treating the Mg-8Li-4Y-2Er-2Zn-0.6Zr alloy for 6 h at 450°C, the fishbone-like

secondary phases at grain boundaries and the granular secondary phases within grains disappeared, while block-shaped secondary phases appeared [126].

Solvent treatment of Mg-Li-Al alloys can increase the matrix Al content and dissolve the AlLi phase. Similarly, at higher temperatures and longer aging durations, the quantity of AlLi phase increases. Rapid cooling in an ice-water combination causes the as-cast Mg-9Li alloy to rapidly transform from its bulk phase into tiny needle-like phases equally dispersed throughout the matrix. This transition occurs after heating the alloy to 575°C for 1.5 h. During this transformation, the phase transitions from body-centered cubic (bcc) to hexagonal close-packed (hcp) [99]. This specific microstructure leads to reduced corrosion and the formation of a surface coating on the β-Li phase, covering the entire alloy surface. Additionally, pitting corrosion is less likely to occur in the alloy. The α-Mg and β-Li phases exhibit almost identical elemental concentration and electrochemical activity due to the decreased atom dispersion in the solid solution, enhancing corrosion resistance [99]. A study [127] showed that the corrosion behavior of Mg-9Li-3Al-2.5Sr alloys under various aging circumstances. Alloys with the greatest corrosion resistance were those heated to 150°C for six hours, as the uniform distribution of the Al4Sr phase along the boundary grain helped to prevent further corrosion damage.

Annealing Mg-Li alloy at low temperatures for a brief time after extrusion or rolling is another method to enhance its corrosion resistance. Partially dynamic recrystallization occurs after one hour of annealing at 200°C in cold-rolled LZ91 sheets due to the significant deformation and thermal energy accumulated during cold rolling [128,129]. Corrosion current density and corrosion pits are reduced because the microstructure is homogeneous and the grains are polished. The resistance of corrosion of as-extruded Mg-7.5Li-3Al-1Zn alloy can be further enhanced by treatment of annealing, which speeds up the diffusion of Li atoms and alters the relative composition of the α-Mg and β-Li phases [39,130]. Increasing the volume of β-Li from 29% to 35% effectively decreases the corrosion current, as it reduces the area ratio of the cathode to the anode for corrosion (galvanic) [57]. According to study by Dobkowska et al. [131], changing the grain size of Mg-Li-Al alloy by the treatment of heat which has no effect on its resistance. Therefore, corrosion is mostly determined by the presence of the second phase. To make Mg-Li-Al alloys more corrosion-resistant, it is essential to anneal the alloy to reduce imperfections, age it to produce beneficial secondary phases, and use solid solution treatment to dissolve detrimental secondary phases.

5 Effect of Aluminum and Lithium Concentration on the Corrosion Behaviour of Mg Alloys

An alloy is formed when a metal is combined with precise quantities of other metallic elements, acquiring distinct properties. This alloying process is highly effective for developing and enhancing the properties of metals.

5.1 Aluminum (Al) Concentration

Materials scientists frequently investigate the Mg-Al family of magnesium alloys. Within this system, two distinct mechanisms—strong solution strengthening and precipitation strengthening—contribute to the reinforcement of magnesium alloys [5,62,132]. Aluminum (Al) plays a crucial role in enhancing the overall quality of magnesium alloys by modifying their grain structure [12,34]. Additionally, a homogenous intermetallic phase called Mg17Al12 can disperse along grain boundaries or dissolve inside grains, resulting from the combination of magnesium and aluminum [133,134]. This intermetallic phase significantly enhances the corrosion resistance of magnesium alloys. Comparing

AE42 and AE21 magnesium alloys reveals that AE42 alloys exhibit a more consistent element distribution and lower grain sizes, suggesting the rapid formation of stabilizing layers rich in aluminum. Consequently, AE42 alloys demonstrate superior corrosion resistance compared to AE21 alloys [135]. Increasing the aluminum content significantly affects the grain structure, as evidenced by experimental observations in Mg-Al-Ca-Mn alloys. At high aluminum concentrations, increased precipitation of secondary phases makes grain expansion more challenging during dynamic recrystallization. The resulting fine-grained structure substantially reduces corrosion with its increased number of grain boundaries [136]. Table 2 presents the corrosion currents and potentials of materials A04, A08, and A12 in a 3.5 wt% NaCl solution, offering valuable insights into their corrosion behavior.

Table 2: Corrosion currents and potentials of A04, A08, and A12 in a 3.5 wt% NaCl solution

Alloy	Composition	Ecorr (V_{SCE})	Icorr ($\mu A/cm^2$)	Yield strength [137]	Tensile strength [137]	Grain size (μm)	Corrosion rate (mm/year)	Reference
A04	Mg-4%Al	−1.671	885.23	150	250	30	1.02	[136]
A08	Mg-8%Al	−1.669	316.65	140	240	25	0.45	[136]
A12	Mg-12%Al	−1.655	212.54	130	230	20	0.30	[136]

5.2 Lithium (Li) Concentration

Research in the field has extensively documented the influence of lithium (Li) concentration on the microstructure and properties of magnesium-lithium alloys (Mg-Li) [32,138]. Varying levels of lithium in Mg-Li alloys lead to the formation of various solid solutions, with the α-Mg phase being the most common at a weight percent of 10.3 lithium [139]. Characteristics of corrosion of Mg-Li alloys are closely linked to their crystal structures, where the concentration of lithium plays a more significant role in corrosion behavior than the type of crystal structure, whether hexagonal close-packed (hcp) or body-centered cubic (bcc) [93]. Table 3 presents corrosion rates for various Mg-Li alloys with different lithium concentrations, revealing that lithium in Mg-Li alloys reduces corrosion current density and inhibits hydrogen formation.

However, corrosion resistance is adversely affected by the β-Li phase, particularly at higher lithium concentrations [57]. Cain et al. [57] have reported that Mg-Li alloys with increased lithium concentrations exhibit superior corrosion resistance. Filiform corrosion is predominantly observed on α-Mg phase surfaces in Mg-4Li and Mg-7.5Li alloys with low lithium concentrations, while Mg-14Li alloy displays less pitting corrosion. Negative difference effect (NDE) experiments indicate that alloys with surface film rupture, such as Mg-4Li and Mg-7.5Li, exhibit increased NDE, whereas alloys with a β-Li phase show decreased NDE due to a persistent surface film [140].

According to Tian et al. [141], the as-extruded LAZ832-0.2Zr alloy demonstrates better corrosion resistance than the LAZ1132-0.2Zr alloy. The α-Mg alloy generates a significant amount of hydrogen gas when Mg-Li alloys with varying lithium contents are utilized as battery anodes, whereas the β-Li alloy notably reduces hydrogen gas emission. According to Wang et al. [142], the Mg-3Al-8Li alloy shows better self-discharge mitigation and more homogeneous dissolving of discharge products compared to Mg-3Al alloys with 12 or 4 wt%. In considering corrosion in Mg-Li alloys with high Li content, it is essential to account for various types of corrosion in the α-Mg and β-Li phases, as well as the impact of oxides, hydroxides, and carbonates on corrosion behavior [143,144]. The lithium

concentration determines the crystal structure of Mg-Li alloys. Alloys containing less than 5.7% Li predominantly exhibit a hexagonal close-packed α-Mg phase. With increasing lithium content, alloys transition to α-Mg and β-Li phases. The β-Li phase, characterized by a bc cubic structure, becomes predominant after 11 weight percent [93,140,145]. The addition of lithium to magnesium enhances its strength and ductility compared to pure magnesium, further strengthened by the creation of protective $Li_2CO_3/MgCO_3$ layers, enhancing anti-corrosion properties [122].

Table 3: Corrosion rates for various Mg-Li alloys with different lithium concentrations

Alloy	State	Li content (wt%)	Solution	Corrosion rate (mm/a)	Observed corrosion features	Inhibits hydrogen formation	Reference
Mg-xLi	As-extruded	7.5	NaCl (0.1 mol/L)	3.381	Mixed filiform and pitting	No	[57]
Mg-xLi	As-extruded	4	NaCl (0.1 mol/L)	1.848	Filiform patterns corrosion	Yes	
Mg-xLi	As-extruded	14	NaCl (0.1 mol/L)	0.861	Pitting with no filiform	Yes	
Mg-3Al-xLi	As-cast	8	NaCl (3.5 wt%)	3381.8	Mild spalling	No	[142]
Mg-3Al-xLi	As-cast	4	NaCl (3.5 wt%)	18956	Severe metallic particles spalling	No	
Mg-3Al-xLi	As-cast	12	NaCl (3.5 wt%)	5300.3	Localized severe pitting	No	

6 Corrosion Types of Mg Alloys

Magnesium exhibits a lower typical electrode potential of −2.37 V than aluminum and lithium. Magnesium readily forms a loose and porous oxide film when exposed to air. This magnesium oxide film protects the primary magnesium less effectively than the Al_2O_3 film on aluminum alloys [146]. Table 4 categorizes the different types of corrosion observed in Mg alloys, providing an overview of the prevalent corrosion mechanisms affecting these materials.

Table 4: Corrosion types of Mg alloys

Corrosion type	Description	Influencing factors	Challenges and considerations	Experimental evidence	References
General corrosion	Gradual dissolution of magnesium alloy surfaces, resulting in the release of electrons (anodic reaction) and formation of a hydroxide film.	Reduction of hydrogen ions or oxygen at the cathode, leading to the formation of water or hydroxide ions (cathodic reaction).	Alloy composition, environmental conditions, solution chemistry	Weakness of protective film, susceptibility to cracking, effects of alloy composition and environment; Hexagonal structure of film	[11,147]
Localized corrosion	Heterogeneous corrosion causes localized anodic dissolution, resulting in localized damage such as pits or filiform corrosion.	Oxygen reduction or formation of concentration cells at cathodic sites, promoting localized corrosion.	Grain size, secondary phases, solution composition, microstructure	Initiation and propagation factors, environmental influence, microstructure's role, pitting and filiform corrosion	[148–150]
Galvanic corrosion	Accelerated anodic dissolution due to electrochemical interaction between magnesium alloy (anode) and dissimilar metal or alloy (cathode).	Reduction of hydrogen ions or oxygen at the cathode, consuming electrons produced by magnesium alloy corrosion (cathodic reaction).	Electrode potential difference, contact area, environmental conditions	Active anodic behavior of magnesium, impact of impurities, challenges in corrosive environments; Corrosion current measurement	[151–153]
Stress corrosion cracking	Cracking under stress induced by anodic dissolution and embrittlement due to hydrogen evolution (anodic reaction) and absorption (cathodic reaction).	Absorption of hydrogen ions or oxygen reduction at cathodic sites, facilitating hydrogen embrittlement and crack propagation.	Stress, anodic dissolution, hydrogen embrittlement, grain size and orientation	Role of stress in initiation and propagation, interaction with secondary phases, grain effects; Crack initiation and propagation	[154–156]

Magnesium alloys degrade quickly in water due to corrosion and the release of hydrogen gas [157]. In the corrosive environment of magnesium, where corrosion primarily occurs, certain areas called cathodic zones are particularly active in promoting corrosion. These zones include impurity particles, regions with high concentrations of noble elements, and secondary phases. As a result of these reactions, the pH around these areas may slightly decrease [158]. The highly negative electrode potential of magnesium makes it susceptible to internal galvanic attack [159]. Additionally, alkaline conditions develop locally at the cathodic sites, leading to pH levels rising to around 10–11. When this rising alkalinity reaches the passivity zone of magnesium, a protective outer layer of magnesium hydroxide ($Mg(OH)_2$) forms, while a dehydrated core layer of magnesium oxide (MgO) develops [160,161]. Furthermore, the inner layer of magnesium-based alloys tends to accumulate atoms of noble elements due to selective corrosion processes favoring the breakdown of active magnesium atoms [157]. Magnesium alloys corrosion is a complex process involving various types, such as general localized, galvanic and stress cracking corrosion. While galvanic corrosion is the most common and magnesium alloys mostly experience stress corrosion cracking.

6.1 General Corrosion

When magnesium alloys are exposed to water and undergo electrochemical reactions, the magnesium matrix gradually dissolves, forming a surface hydroxide film and releasing hydrogen gas [147]. This process, known as general corrosion, is characterized by uniform deterioration across the material's surface. The resultant film layer displays a hexagonal structure [11], wherein hydroxide and magnesium ions are arranged alternately within the crystal lattice. However, the bonding between these ions is relatively weak, making the film susceptible to cracking and providing limited protection to the underlying substrate. Despite its uniform nature, general corrosion is typically considered less damaging to alloys of magnesium than other corrosion forms [147]. The specific general product corrosion of a magnesium alloy is influenced by both its chemical composition and environmental factors that contribute to corrosion.

6.2 Local Corrosion

Localized corrosion, including pitting and filiform corrosion, presents a more significant risk to magnesium alloy substrates than general corrosion due to the heterogeneous corrosion rates observed across various regions [162,163]. Pitting corrosion arises when the protective surface film is ruptured, exposing the substrate to the corrosive environment and initiating localized corrosion processes [148]. Factors such as grain size, solution chemistry, alloy composition, and the presence of secondary phases significantly influence the occurrence of pitting corrosion. Smaller grain sizes typically correlate with reduced susceptibility to pitting corrosion [149]. Magnesium alloys are notably prone to corrosion in saline environments, particularly those containing chloride ions (Cl^-), which can infiltrate surface coatings and trigger localized electrochemical corrosion, thereby promoting pitting corrosion [164]. Moreover, the pH of the solution plays a role in the start of pitting corrosion, with alkaline conditions ($pH > 10.5$) generally impeding its onset. Filiform corrosion, conversely, typically manifests beneath surface oxide layers and protective coatings [150]. This phenomenon is influenced by various factors, including the corrosive environment, microstructure, composition of oxide layers, and defects within the naturally occurring oxide layer on the alloy surface. Precipitates and alloying elements' distribution within the material can serve as nucleation sites for corrosion, leading to its propagation in diverse directions. The microstructure of the alloy plays a pivotal role in filiform corrosion, where the potential difference between the cathodic tail and the anodic head acts as the driving force for its expansion [165]. A study suggested that when alloys of magnesium are exposed to a NaCl aqueous solution,

filiform corrosion originates from second-phase particles accumulated along grain boundaries and propagates along these boundaries [166]. Notably, the microstructure significantly influences the pattern of filiform corrosion, with observations indicating its predominant occurrence and expansion within the $\alpha + \beta$ phase of layered structures. Grains within the α phase exhibit fewer filiform corrosion, while no filamentary corrosion is observed within the β-phase [167].

6.3 Galvanic Corrosion

Galvanic corrosion, also recognized as bimetallic or contact corrosion, is an electrochemical phenomenon arising from the contact or immersion of two dissimilar metals or alloys with distinct electrode potentials [151,152]. In such scenarios, the metal with a lower electrode potential typically experiences accelerated corrosion, while the one with a higher potential corrodes slower. The degree of galvanic corrosion is primarily contingent upon the variance in electrode potentials between the involved metals [153]. Due to their relatively low corrosion potential, Mg alloys often serve as active anodes in galvanic couples, rendering them susceptible to preferential corrosion within such systems. Studies suggest a direct correlation between the rate of galvanic corrosion and the ratio of cathodic area to anodic area. With an increase in this ratio, the current density escalates, consequently augmenting corrosion rates [152]. The galvanic corrosion relationship between Mg alloys and other metals is influenced by effective contact area, electrode potential, and prevailing environmental conditions. The utilization of magnesium alloys in environments containing active chemicals poses challenges due to their vulnerability to galvanic corrosion. Within magnesium alloys, the presence of secondary phases and impurities introduces varied electrochemical activities, leading to the formation of micro-scale thermocouples. In corrosion, secondary phases or impurities frequently act as cathodes, while the Mg-rich phase acts as the anode due to its lower potential. This setup forms a galvanic couple, resulting in the generation of a corrosion current. The damage caused by galvanic corrosion correlates with the magnitude of the corrosion current flowing between these galvanic couples [168].

This relationship can be quantified using equation:

$$I_{galvanic} = (E_{pc} - E_{pa})/(R_m + R_c) \tag{21}$$

where:

- $I_{galvanic}$ represents the galvanic corrosion current.
- E_{pc} denotes the cathodic potential of polarization.
- E_{pa} signifies the anodic potential of polarization.
- R_m represents the metal resistance.
- R_c denotes the electrolyte resistance.

Enhancing the corrosion resistance of magnesium alloys is a key objective in materials science, particularly through modifications in the corrosion (galvanic) dynamics between the magnesium matrix and the second phase. Recent investigations have highlighted the potential of Mg-RE-TM alloy systems to significantly improve mechanical properties, incorporating transition metals and rare earth elements in optimized proportions. The notable improvement observed in corrosion resistance is primarily attributed to a long-period stacking ordered (LPSO) structure within the second phases of magnesium alloys [169,170]. While the 18R and 14H LPSO structures are the most commonly observed, other phases such as 10H, 12H, 14H, 15R, 18R, 21R, and 24R also exist [170]. Despite significant advancements, a challenge known as micro-galvanic corrosion persists between the cathodic LPSO and anodic α-Mg phases. An in-depth investigation of the 18R-LPSO phase in magnesium

alloys ZWM120, ZWM240, and ZWM480 revealed that an increased LPSO volume leads to reduced corrosion resistance under galvanic corrosion conditions [171].

Further research [172,173] suggested that VN3 Mg alloys, which have higher volume fractions of LPSO 18R phases, demonstrate enhanced resistance to corrosion compared to VN1.5 alloys. This improvement is primarily attributed to a continuous network of compacted LPSO phases in VN3 alloys, which inhibits corrosion growth at higher volume fractions. Conversely, alloys containing both 14H and 18R LPSO structures exhibit inferior corrosion resistance, indicating that magnesium-yttrium-zinc (Mg-Y-Zn) alloys featuring a single LPSO structure, such as 14H or 18R, may offer better corrosion resistance [174]. Despite the importance of these findings, further investigation into the corrosion behavior of magnesium alloys in the presence of the LPSO phase is warranted. These studies will contribute to a deeper understanding of the underlying mechanisms and aid in developing strategies to enhance the corrosion resistance of magnesium alloys in practical applications.

6.4 Stress Corrosion Cracking (SCC)

SCC arises in Mg alloys when they corrode due to environmental factors, leading to the development, elongation, and eventual spread of fractures under stress [154]. Two primary perspectives on SCC in magnesium alloys are recognized: hydrogen embrittlement and anodic dissolution mechanisms. As per the anodic dissolution theory, stress induces the slipping and rupture of the surface film on magnesium alloys. Consequently, the exposed matrix behaves as an anode compared to the surface film, causing rapid dissolution and continuous corrosion through electrochemical processes [155]. Conversely, the hydrogen embrittlement theory suggests that hydrogen produced during the magnesium alloy corrosion permeates the matrix and congregates at crack tips. When a critical concentration is attained, cracks initiate, elongate, and propagate [156]. Considering the inevitability of stress in practical applications of magnesium alloys, investigations into the AZ91 magnesium alloy corrosion process under varied stress levels have unveiled that while the initial corrosion product forms a protective layer, hindering direct interaction between the corrosive medium and the magnesium alloy matrix, the application of stress facilitates the corrosion pits formation. These pits allow corrosive substances to penetrate the substrate, quickening corrosion [175]. Stress corrosion cracking (SCC) typically occurs due to localized corrosion, and the presence of second-phase particles within the alloy increases its susceptibility to this type of corrosion. The rapid matrix dissolution adjacent to these particles and the detachment of the particles themselves contribute to extensive corrosion cracks. Moreover, grain size and orientation differences govern the crack propagation directions during SCC [137,176].

7 First Principle Calculation of Mg-Al-Li Alloys

7.1 Mechanical Properties

Determining elastic constants is paramount in evaluating a crystal's resilience against external stressors and offers valuable insights into the bonding dynamics near equilibrium conditions [177]. Exploring these constants is indispensable for comprehending the mechanical behavior across different phases. Traditionally, alterations in a system's volume exert a more pronounced effect on its total energy than strain-induced changes. Nevertheless, methods employing volume-conserving strains can mitigate the influence of volume variations on the total energy [178]. For cubic crystal structures such as $Mg_{17}Al_{12}$ and Mg_2Li, only three independent elastic constants are pertinent: C_{11}, C_{12}, and C_{44}. These constants serve as foundational descriptors for delineating the elastic properties of these phases. Such data stands as a cornerstone for advancing the understanding of the mechanical attributes of these

materials and their prospective applications. A comparative analysis has been conducted between the Cauchy pressure (AZ), elastic constants (Cij), and anisotropic properties (AE) for the Mg-Al and Mg-Li phases, compared against values reported in extant literature. For the Mg-Al phase, the study reports C_{11}, C_{12}, and C_{44} values of 90.5, 26.7, and 29.7 GPa, respectively, with a C_{12}–C_{44} difference of −3.0 GPa, AZ of 0.93, and AE of 0.07. Another study calculations by [179] (88.38, 23.54, 26.95 GPa, respectively, with a C_{12}–C_{44} difference of −3.41 GPa). Other studies have also reported similar values [180] (89.86, 27.21, 33.32 GPa, with a C_{12}–C_{44} of −6.11 GPa), while Reference [181] found values of (97.7, 28.1, 31.4 GPa). Additionally, Reference [182] lists values of (70.58, 25.35, and 30.31 GPa, with a C_{12}–C_{44} of −4.9 GPa and an AZ of 1.34). Experimental values from [183] indicate slightly different results, with (82.4, 20.8, and 36.6 GPa, showing a more significant C_{12}–C_{44} difference of −15.8 GPa and an AZ of 1.19). For the Mg_2Li phase, Zhang et al. calculations reported values of (69.8, 25.9, and 31.1 GPa, with a C_{12}–C_{44} difference of −5.2 GPa). $Mg_{17}Al_{12}$ and Mg_2Li phases are mechanically stable, satisfying cubic crystal's corresponding mechanical stability conditions [184].

The precision of elastic constants can be significantly influenced by the reciprocal-space mesh utilized for integrating across the Brillouin zone, with discrepancies often linked to variations in the k-point sampling. In their investigation, De Boor et al. [185] explored the impact of temperature fluctuations on the elastic constants of Mg_2Li employing the quasi-harmonic approximation, observing that C_{12} experiences the most pronounced alterations in response to temperature variations. Specifically, the elastic constant C_{11} quantifies the material's resistance to linear compression along the x-direction. The Cauchy pressure, denoted as C_{12}–C_{44}, elucidates the angular nature of atomic bonding in both compounds and metals [186]. A negative Cauchy pressure indicates directional bonding, a characteristic frequently observed in nonmetallic materials, while a positive value suggests metallic bonding. Notably, research by Wang et al. [187] indicated Cauchy pressures of −3.0 GPa and −4.1 GPa for Mg-Al and Mg-Li phases, respectively, indicative of their intrinsic brittleness akin to many non-metals. Anisotropic behavior in cubic crystals can be quantified by the parameter AE and Zener anisotropic index (AZ) [188].

$$A_Z = 2C_{44}/(C_{11} - C_{12}) \tag{22}$$

$$A_E = (C_{11} - C_{12} - 2C_{44})/(C_{11} - C_{44}) \tag{23}$$

The comprehension of mechanical properties in polycrystalline Mg-Li-Al phases necessitates a thorough understanding of shear modulus (G), isotropic bulk modulus (B), Poisson's ratio (ν) and Young's modulus (E). To derive these properties, the Voigt-Reuss-Hill (VRH) methodology is employed. This approach offers a framework to approximate the effective moduli of polycrystalline materials by aggregating upper (Voigt) and lower (Reuss) bounds of elastic constants.

In the context of a cubic crystal system, the limits of shear modulus (G) and bulk modulus (B), known respectively as Voigt and Reuss bounds, can be articulated as follows according to established literature [189]:

Voigt bounds

$$B_V = \frac{C_{11} + 2C_{12}}{3} \tag{24}$$

$$B_V = \frac{C_{11} - C_{12} + 3C_{44}}{5} \tag{25}$$

Reuss bounds

$$B_R = \frac{(C_{11} + 2C_{12})(C_{11} - C_{12})}{C_{11} + 2C_{12} + 2(C_{11} - C_{12})} \tag{26}$$

$$G_R = 5[4(\mathrm{C}_{11} - \mathrm{C}_{12}) + 3\mathrm{C}_{44}]^{-1} \tag{27}$$

The Hill average is the arithmetic mean of the Reuss and Voigt bounds:

$$B_H = \frac{CB_v + B_R}{2} \tag{28}$$

$$B_H = \frac{B_v + G_R}{2} \tag{29}$$

Using the Hill averages, Poisson's ratio (ν) and Young's modulus (E) are calculated as follows:

$$E = \frac{9B_H G_H}{3B_H + G_H} \tag{30}$$

The elastic moduli serve as pivotal metrics for assessing material hardness. The bulk modulus (B) delineates a material's capacity to resist volume alterations under pressure, while the shear modulus (G) signifies its ability to withstand alterations in shape [190]. Young's modulus (E), the ratio of stress to strain, furnishes insights into a material's rigidity, with higher values indicating greater stiffness [191]. Notably, research by Xue et al. [192] indicated that the Young's modulus of Mg-Al surpasses that of Mg-Li, suggesting that Mg-Al exhibits greater stiffness.

The Young's modulus aids as a visual appearance of a material's anisotropic attributes. For cubic systems, understanding these directional dependencies necessitates familiarity with the theoretical expressions governing Young's modulus (E). To elucidate the anisotropic characteristics, 3D surface contours of Young's modulus for Mg-Al and Mg-Li are presented. These expressions for cubic systems are articulated as follows:

$$E(\theta, \phi) = \left[S_{11} - 2\left(S_{11} - S_{12} - \frac{1}{2} S_{44} \right) \left(\cos^2\theta \cos^2\phi + \cos^2\theta \sin^2\phi + \sin^2\theta \right) \right]^{-1} \tag{31}$$

where:

- S_{ij} are the compliance coefficients.
- θ and ϕ are the polar and azimuthal angles, respectively.

Fig. 4 displays the relationship between strain (εx) and various mechanical properties: (a) Bulk modulus (B), (b) Shear modulus (G), (c) Young's modulus (E), and (d) Poisson's ratio (μ), illustrating their respective behaviors under strain.

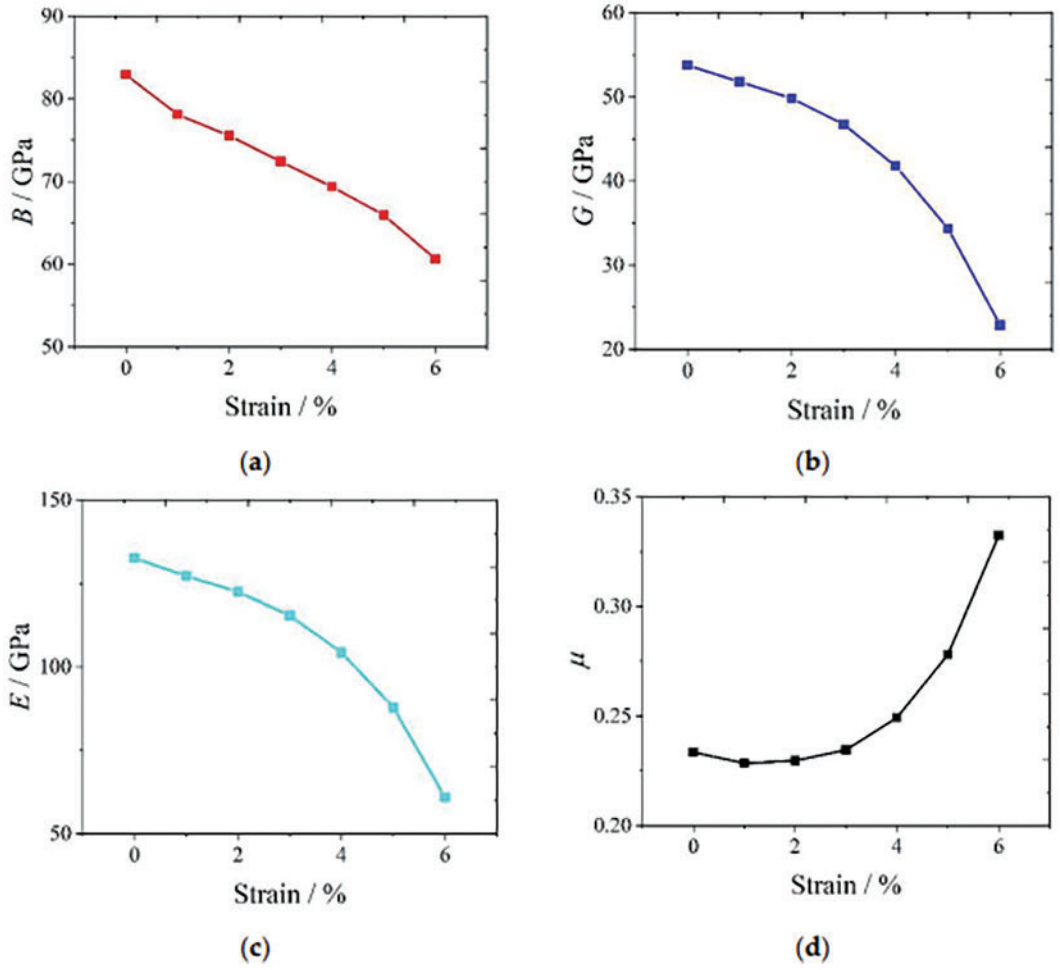

Figure 4: (a) Bulk modulus B *vs.* strain ε_x; (b) Shear modulus G *vs.* strain ε_x; (c) Young's modulus E *vs.* strain ε_x; (d) Poisson ratio μ *vs.* strain ε_x

Orhan et al. [193] introduced the pugh ratio concept that the ratio of bulk to shear modulus (B/G) serves as a common metric for assessing the brittleness or ductility of materials. A higher B/G ratio signifies a ductile response, while a lower ratio indicates a brittle behavior. The threshold value distinguishes between ductile and brittle materials at 1.75. Moreover, previous research [194,195] highlighted the significance of Poisson ratio in characterizing a crystal's resistance to shear deformation, typically ranging from −1 to 0.5. Elevated Poisson's ratios indicate superior plasticity, with values surpassing 1/3 indicative of ductile characteristics and those falling below 1/3 suggesting brittleness. In another study, Poisson's ratios below 1/3 further corroborate the brittle attributes of Mg-Li-Al alloys [196]. First-principle calculations of Mg-Al-Li alloys indicate that increased mechanical strength enhances corrosion resistance. Higher strength reduces microcrack formation and propagation, while refining the alloy's microstructure. This results in fewer grain boundaries and more uniform protective oxide layers, which together help to resist corrosive agents and prevent stress corrosion cracking. Fig. 5 shows the Poisson's ratio and Pugh ratio of the Mg-Li-Al alloy.

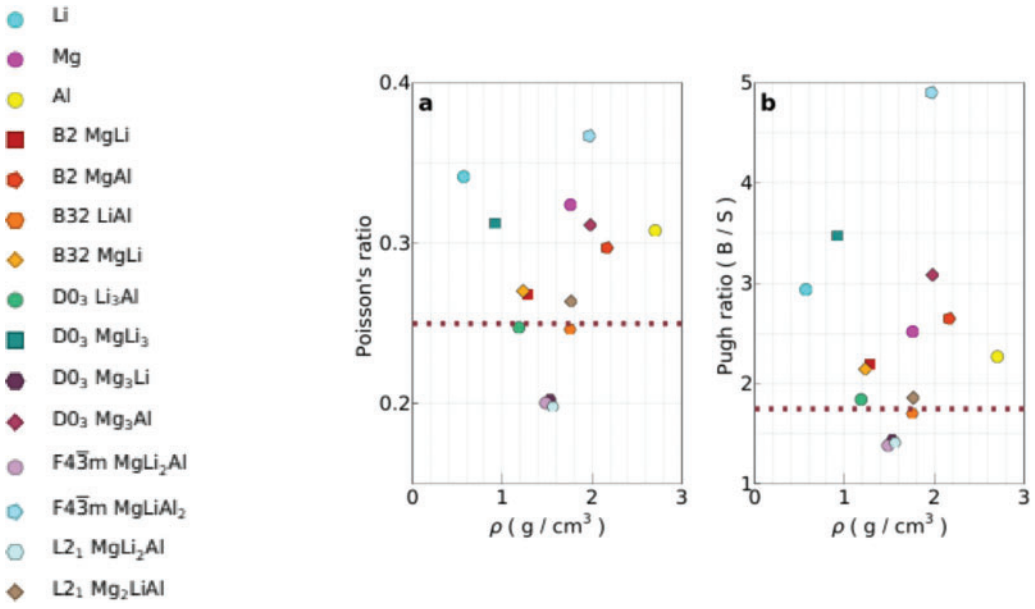

Figure 5: Poisson's ratio and Pugh ratio of Mg-Li-Al. Reprinted/adapted with permission from Reference [193]. Copyright 2022

7.2 Debye Temperature and Sound Velocity

The determination of phase velocities for pure longitudinal and transverse modes within the Mg-Li-Al phases can be achieved by using single-crystal elastic constants in conjunction with Christoffel equation resolution [193]. Prior investigations explained that the determination of sound velocities is depending upon the symmetry of the crystal and the direction of propagation. Specifically, in cubic crystals, the calculation of sound velocities for both transverse and longitudinal waves across three unique crystal orientations—[1 1 0], [1 0 0], and [1 1 1]—was accomplished utilizing the equation provided in Reference [197]:

$$\begin{aligned} &V_{\mathrm{T1}}^{[100]} = V_{\mathrm{T2}}^{[100]} = \sqrt{C_{44}/\rho},\ V_{\mathrm{L}}^{[100]} = \sqrt{C_{11}/\rho}, \\ &V_{\mathrm{T1}}^{[10]} = \sqrt{C_{44}/\rho},\ V_{\mathrm{T2}}^{[110]} = \sqrt{(C_{11}-C_{12})/\rho},\ V_{\mathrm{L}}^{[110]} = \sqrt{(C_{11}+C_{12}+2C_{44})/2\rho}, \\ &V_{\mathrm{T1}}^{[111]} = V_{\mathrm{T2}}^{[111]} = \sqrt{(C_{11}-C_{12}+C_{44})/3\rho},\ V_{\mathrm{L}}^{[111]} = \sqrt{(C_{11}+2C_{12}+4C_{44})/3\rho}. \end{aligned} \tag{32}$$

Phases with lower density and higher elastic constants exhibit greater sound velocities [198,199]. A study by Fu et al. [200] highlighted that longitudinal waves attain their maximum speed along the [1 0 0] direction for Mg-Al and along the [1 1 1] direction for Mg-Li. These variations in sound velocities highlight the elastic anisotropy inherent in both phases. The sound velocity prediction across different crystallographic directions for both materials represents an initial endeavor [201].

The Debye temperature (ΘD) is important in understanding various solid-state physics phenomena, including lattice vibrations, thermal conductivity, and specific heat. Additionally, unlike molecular weight, it provides valuable information about the bonding strength present within a crystal lattice. In determining the Debye temperature for the Mg-Li-Al system, researchers utilize the average

sound velocity (Vm), as outlined in the equation [202]:

$$\Theta_{\mathrm{D}} = \frac{h}{k_{\mathrm{B}}}\left[\frac{3n}{4\pi}\left(\frac{N_{\mathrm{A}}\rho}{M}\right)\right]^{\frac{1}{3}} V_{\mathrm{m}}, \tag{33}$$

The factors here consist of Planck's constant (h), Boltzmann's constant [175], Avogadro's number (N_A), molecular weight (M), mass density (ρ), and the no. of atoms per formula unit (n). By utilizing this equation, one can calculate the avg wave velocity (V_m) of a polycrystalline material [203]:

$$V_{\mathrm{m}} = \left[\frac{1}{3}\left(\frac{2}{V_{\mathrm{t}}^3} + \frac{1}{V_{\mathrm{t}}^3}\right)\right]^{-\frac{1}{3}}, \tag{34}$$

Using Hill's shear (G) and bulk modulus (B) in Navier's equation allows us to determine the transverse (V_t), longitudinal (V_l) sound velocities of a material [204]:

$$V_{\mathrm{t}} = \sqrt{\frac{G}{\rho}}, V_{\mathrm{t}} = \sqrt{\left(B + \frac{4}{3}G\right)/\rho}. \tag{35}$$

Recent research findings have demonstrated a positive correlation between Debye temperature and thermal conductivity, indicating that materials with higher Debye temperatures exhibit greater thermal conductivity. The measured ΘD value for Mg-Li-Al surpasses that of other metallic counterparts, indicating its superior thermal conductivity and enhanced chemical bonding characteristics [55]. Higher Debye temperature and sound velocity in Mg-Al-Li alloys indicate greater atomic bonding strength and elastic stiffness, respectively. These properties enhance corrosion resistance by reducing atomic vibrations and preventing microstructural defects, thereby improving the integrity of protective oxide layers and mitigating pathways for corrosive agents. Fig. 6 depicts the temperature-dependent energy (G), illustrating how energy varies with changes in temperature.

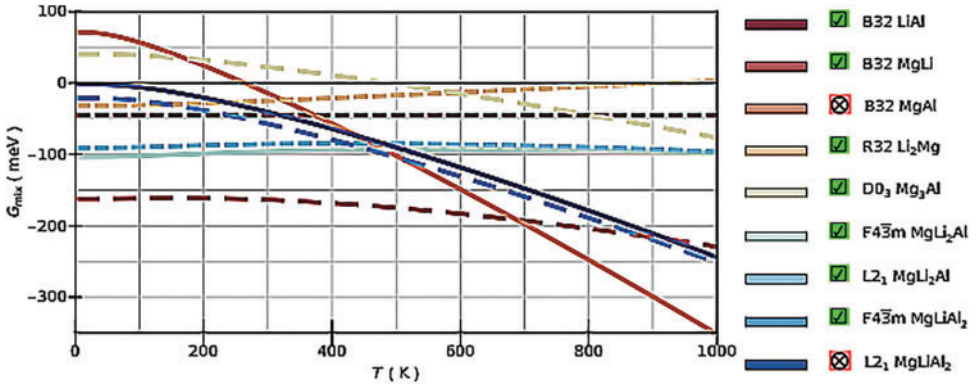

Figure 6: Temperature-dependent energy (G). Reprinted/adapted with permission from Reference [193]. Copyright 2022

7.3 Electronic Structure

In examining the structural stability and bonding attributes of Mg-Li-Al, an analysis of the partial density of states (PDOS) and the total density of states (TDOS) in proximity to the Fermi level was directed [205,206]. The Fermi level (EF) serves as the reference point, with zero energy corresponding to it. Recent studies [207,208] have revealed the presence of multiple energy states intersecting the

Fermi level within the DOS structures, indicative of metallic behavior. The primary peaks in bonding for Mg-Al within the lower energy spectrum are primarily attributed to the Al 3s states, with a minor contribution from Mg 3s and Al 3p states. Al 3p and Mg 2p states predominate close to the Fermi level, suggesting that the metallic behavior is closely linked to the p states of Al or Mg atoms. The observed hybridization between Al and Mg states suggests the presence of bonding similar to covalent interactions in the Mg-Al phase.

Further studies [209,210] stated TDOS for Mg-Li reveals two discernible regions below the Fermi level (0 eV). The first region, spanning from −10 to −5.0 eV, is largely influenced by Li 5s states with some contribution from Mg 3s states, exhibiting strong hybridization between Mg 3s and Li 5s states. In the region spanning from −5.0 eV to the Fermi level, the dominant states are primarily associated with Li 5p states. Additionally, interactions between Mg s-p and Li s-p states are observed above the Fermi energy level. The Mg-Li system exhibits the characteristic small band gap typical of semiconductor materials with a predicted total density of states (TDOS) value of only 0.363 electrons per electron volt per formula unit (eV-1 f.u.-1). Wang et al. [211] have reported a lower number of bonding electrons per atom for Mg-Al compared to Mg-Li, suggesting greater stability for Mg-Li due to a higher number of bonding electrons. Mulliken population analysis by Li et al. [212] indicates electron transfer from Mg atoms to Al and Li atoms in Mg-Li-Al, indicating an ionic nature. This relative electron transfer serves as a qualitative parameter for system characterization. Additionally, bond population analysis, as utilized by another study [213], provides an objective and quantitative measure for assessing bond character. A value of −2 indicates an anti-bonding state, while a value of 1 signifies increasing degrees of covalency. A value of 0 suggests no bonding. The electronic structure analysis reveals that bonding in Mg-Li-Al encompasses a combination of covalent, ionic, and metallic characteristics, with Mg-Li-Al bonds exhibiting a higher degree of covalence than other metallic bonds [214]. The electronic structure of Mg-Al-Li alloys, characterized by metallic behavior and covalent bonding, influences corrosion resistance. Stronger covalent bonds and significant electron transfer enhance the stability of the alloy's surface, reducing susceptibility to corrosive agents and supporting the formation of durable protective oxide layers.

7.4 Thermodynamic Properties

DFT-based first-principles calculations conventionally operate under absolute zero temperature (T = 0 K), a restriction that also extends to phonon analyses. These computations play a pivotal role in deducing the thermodynamic attributes of materials, encompassing temperature-dependent variables such as entropy (S(T)), free energy (G(T)), enthalpy (E(T)), and constant volume heat capacity (CV(T)). To evaluate these properties for the Mg-Li-Al compound, the PHDOS covering both partial and cumulative aspects is assessed at the theoretical equilibrium volume [205]. Research conducted by Li et al. [215] highlights that the peaks observed in the PHDOS of Mg-Li-Al predominantly arise from the interactions among Mg, Li, and Al atoms. Notably, Mg atoms exhibit slightly greater contributions than Li and Al atoms. Additionally, findings from another study [216] emphasize the prominence of peaks in the low-frequency domain (around 4 THz), primarily attributable to Mg atoms movements. These varied contributions from constituent atoms are influenced by their discrepancies in mass. The outcomes of PHDOS analysis facilitate determining the system's vibrational free energy. Subsequently, employing the quasi-harmonic approximation (QHA) [217], one can evaluate the thermodynamic parameters vibrational contributions, including enthalpy, entropy, free energy (Helmholtz), and constant volume heat capacity.

The enthalpy in QHA are provided as follows [217]:

$$E(T) = E_{\text{tot}} + E_{\text{zp}} + \int \frac{\hbar\omega}{\exp\left(\frac{\hbar\omega}{k_{\text{B}}T}\right)} F(\omega)\,\mathrm{d}\omega \tag{36}$$

The equation for E_{tot} defines the total of electronic energy, while E_{zp} signifies the zero-point vibrational energy. Moreover, the symbol ħ denotes constant of Plancks (h/2π), and $F(\omega)$ represents the PHDOS.

The computation of F(ω) and E_{zp} can be performed utilizing the expressions provided in [218]:

$$F(\omega) = \frac{1}{N}\int_{BZ}\sum_{j}\delta\left[\omega - \omega_j(\overline{q})\right]\mathrm{d}\overline{q}$$

$$E_{\text{zp}} = \frac{1}{2}\int F(\omega)\,\hbar\omega\mathrm{d}\omega \tag{37}$$

Then, the free energy is given by [219]:

$$G(T) = E_{\text{tot}} + E_{\text{zp}} + k_{\text{B}}T\int F(\omega)\ln\left[1 - \exp\left(-\hbar\omega/k_{\text{B}}T\right)\right]\mathrm{d}\omega \tag{38}$$

The entropy can be obtained as follows [220]:

$$S(T) = k_{\text{B}}\left\{\int \frac{\hbar\omega/k_{\text{B}}T}{\exp\left(\hbar\omega/k_{\text{B}}T\right) - 1}F(\omega)\mathrm{d}\omega - \int F(\omega)\ln\left[1 - \exp\left(-\hbar\omega/k_{\text{B}}T\right)\right]\mathrm{d}\omega\right\} \tag{39}$$

The heat capacity is given by [17]:

$$C_{\text{V}}(T) = k_{\text{B}}\int \frac{\left(\hbar\omega/k_{\text{B}}T\right)^2\exp\left(\hbar\omega/k_{\text{B}}T\right)}{\left[\exp\left(\hbar\omega/k_{\text{B}}T\right) - 1\right]^2}F(\omega)\mathrm{d}\omega \tag{40}$$

According to a study conducted by Guo et al. [205], the computed values of entropy, free energy, enthalpy, and heat capacity for Mg-Li-Al, utilizing the Quasi-Harmonic Approximation (QHA), vary with temperature. These calculations are performed under zero pressure conditions, where the Helmholtz free energy equals the Gibbs energy. The entropy (S) and enthalpy (E) for Mg-Li-Al increase gradually as temperature rises, while the free energy (G) decreases with increasing temperature. Another study by Xin [56] emphasized that the entropy of Mg-Li-Al begins at zero at 0 K and increases rapidly as the temperature exceeds 300 K. The current entropy values are consistent with those presented in a study by Zhang et al. [181], which showed minimal differences between Gibbs energy (G) and calculated entropy with and without contributions of thermal electronic. Another study indicated that the computed Gibbs energy is -6.06 kJ mol^{-1} at 300 K, which aligns with values reported in [17]. Fig. 7 presents a graph showing the variation of enthalpy, Gibbs free energy, and entropy as a function of temperature in a crystalline solid, providing insight into the thermodynamic behavior of the material.

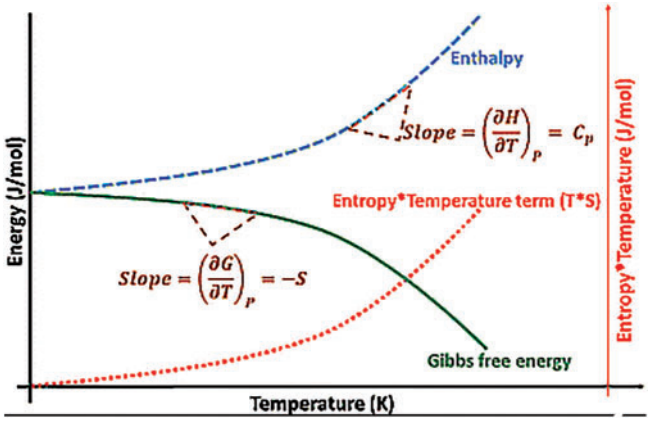

Figure 7: Graph showing enthalpy, Gibbs free energy, and entropy change with temperature in a crystalline solid. Reprinted/adapted with permission from Reference [221]. Copyright 2018

The capacity of heat is a significant thermodynamic parameter that provides valuable information regarding the materials vibrational characteristics. This study investigates the temperature-dependent variations in heat capacity at constant pressure (CP) and constant volume (CV) for Mg-Li-Al over a temperature range of 0 to 1000 K. The findings reveal that CV experiences a notable increase with temperature up to 300 K, following Debye's law. Beyond this temperature, CV stabilizes, exhibiting minimal dependence on temperature and converging towards the 3 NR, where R signifies the ideal gas constant and N represents the total number of atoms in the cell and Dulong–Petit limit. The results indicate that CP values, as computed by Zhang et al. [181], demonstrate slight differences with and without contributions of thermal electronics. At lower temperatures, CP closely parallels CV; however, at higher temperatures, CP exceeds CV due to the impact of thermal expansion. Notably, experimental data on the heat capacity of Mg-Li-Al are lacking in many studies. Thus, these predictions serve as valuable guidance for future theoretical and experimental investigations across various temperature ranges. Thermodynamic properties, such as heat capacity, and enthalpy, influence corrosion resistance in Mg-Al-Li alloys. Higher Debye temperatures and stable thermodynamic profiles enhance structural stability and reduce atomic mobility, leading to more robust protective oxide layers and improved resistance to corrosive environments.

8 Factors that Influence the Corrosion Behaviour of Mg-Li-Al Alloys

8.1 Grain Size

Several studies have investigated the relationship between grain size and corrosion properties in alloys, particularly magnesium and magnesium alloys [222]. Grain refinement is crucial for enhancing corrosion resistance as it increases the density of grain boundaries, making it easier to form a protective coating and ensuring better adhesion of the oxide layer to the substrate. However, there is a debate about whether smaller grains accelerate corrosion due to increased active defects at grain boundaries. Moreover, grain refinement can form isolated cathodes along grain boundaries, facilitating micro-galvanic corrosion. Various casting techniques and processing steps are employed to modify the grain size of Mg-Li alloys [223,224]. Wu et al. [225] demonstrated the impact of grain size reduction by using a rapid solidification technique to produce Mg-13Li-X alloys with fine-grained structures. This resulted in a substantial decrease in grain size, from 150 μm in the traditional as-cast alloy to 4.2 μm. The alloy with smaller grains exhibited a Ecorr of −1.354 V and a corrosion current density of 5.830 ×

10^{-7} A/cm^2 after immersion in Hank's Balanced Salt Solution (HBSS) for two hours. Grain refinement also enhances the corrosion resistance of Mg-Li-Al alloys. A delicate spherical shape can be achieved by incorporating ultrasonic vibration into the melt solidification process, transforming the coarse flower-like structure of the α-Mg phase and reducing corrosion current density and corrosion product production [226].

Comparing the Mg-9Li-3Al-1Ca alloys microstructure, cast by centrifugal casting and gravity casting revealed that the latter method significantly reduced the corrosion current density by refining and spheroidizing the α-Mg phase [227]. Research [228] has demonstrated that improving the grain structure effectively prevents corrosion cracks from penetrating the alloy, thereby reducing the corrosion rate and transforming the corrosion pattern from localized to uniform. Friction stir treatment significantly enhanced the surface finish of Mg-9Li-1Zn alloy grains, reducing corrosion current density and forming numerous small, shallow pits instead of large, deep holes. Generally, reducing grain size improves the corrosion resistance of Mg-Li-Al alloys. Adding half a nanometer of nitrogen to the LAZ832 alloy transforms the equiaxed α-Mg phase into a lengthy ribbon structure, enhancing corrosion resistance despite increasing grain size [229]. Aging temperature also affects corrosion resistance, with higher temperatures leading to larger grain size and improved corrosion resistance in Mg-9Li-3Al-2.5Sr alloys [230]. Moreover, the behavior of corrosion changes with increasing grain size due to the rapid growth of passivation layers and segregation of impurities at grain boundaries. Gao et al. [231] observed uneven distribution of grain sizes within the alloy can affect its corrosion performance. Additionally, the finer grain structure in the top layer of as-extruded Mg-1Li-1Ca alloy exhibited greater corrosion resistance [232]. The following equation can be utilized to elucidate the correlation between grain size and corrosion rate. Similar to the Hall-Petch equation, the rate of corrosion (CR) [233] can be expressed as:

$$CR = a + bD - 0.5 \tag{41}$$

The parameter denoted as D denotes the grain dimensions, whereas the parameters a and b pertain to additional influencing factors. Typically, diminishing the grain dimensions enhances the corrosion resistance of Mg-Li-Al alloys. Nevertheless, there exists a scarcity of comprehensive data concerning intergranular corrosion within Mg-Li-Al alloys, with sporadic investigations into the association between grain size and corrosion resilience in ternary Mg-Li-Al alloys.

8.2 Second Phase

The role of secondary phases significantly influences the corrosion behavior of magnesium alloys, often triggering galvanic corrosion between the matrix and these secondary phases [234,235]. Typically, secondary phases act as cathodes compared to the matrix, accelerating the corrosion rate. Phases like Al-Fe and Al-Mn can drastically increase the corrosion rate of the Mg matrix when serving as cathodes. An intriguing secondary phase known as $Mg_{17}Al_{12}$, found at grain boundaries of AZ alloys, serves a dual role: acting as a cathode to promote hydrogen evolution and as a barrier to protect the material from corrosion. The impact of the $Mg_{17}Al_{12}$ phase depends on its volume fraction and distribution within the alloy microstructure. Elements like La, Nd, and Y facilitate the formation of secondary phase anodes, which are more prone to degradation [236,237].

As previously mentioned, Mg-Li-Al alloys feature typical secondary phases in regular Mg alloys and phases containing Li. Galvanic corrosion processes are common in Mg-Li alloys due to the electrochemical mismatch between the α-Mg and β-Li phases. The local potential distribution around

the α-Mg and β-Li interface and the internal β-Li phase at grain boundaries indicates micro-galvanic corrosion to some extent [57]. Additionally, the structure and composition of the α-Mg phase significantly influence the corrosion dynamics of Mg-Li-Al alloys. The AlLi phase, present in Mg-Li and Al alloys, due to lithium's higher electronegativity compared to magnesium and aluminum, increases the susceptibility of the Mg matrix to galvanic corrosion dissolution [39,238]. Filiform corrosion often extends along the AlLi phase in Mg-Li alloys, with the $\ddot{v}$-Li phase and grain boundaries being common sites for this phenomenon. Moreover, the corrosion properties of Mg-Li-Al alloys are influenced by the quasicrystal phase and the long-period stacking ordered (LPSO) phase. Reference [239] discovered that the I phase at grain boundaries in Mg-6Li-6Zn-1.2Y alloys effectively prevents the formation and development of corrosion pits and filiform corrosion, thereby slowing down the corrosion process. Li et al. [240] studied the microstructure and corrosion behavior of Mg-6.5Li-xY-yZn alloys during extrusion. They found that certain compositions effectively decrease micro-galvanic corrosion and have the least second phase, such as the Mg-6.5Li-0.8Y-0.3Zn alloy. This alloy acts as a barrier between the eutectic phase and the matrix.

The ability of secondary phases to resist corrosion is governed by several key factors, including their quantity, structure, potential gradient relative to the substrate, and surface protection function [241]. The potential differences between particles and matrix affect the corrosion rate in LA83-1.2M alloys containing Al_2Gd/Mg_2Sn/AlCuMg particles. This study comparing the relative potential differences of elements in these alloys revealed significant variations, with AlCuMg showing about 680 mV, AlLi approximately 340 mV, Al_2Gd around 250 mV, β-Li about 135 mV, and Mg_2Sn roughly 60 mV. The addition of more noble AlCuMg particles can reduce mass loss by approximately 70% by forming micro-galvanic couples with Al_2Gd and α-Mg, which have smaller potential differences [242]. Altering the solution treatment time in Mg-3Nd-1Li-0.2Zn alloys affects the size and quantity of the Mg41Nd5 secondary phase, leading to the formation of smaller, shallower pitting pits after six hours of treatment at 535°C [243]. Additionally, in cross-cold rolled Mg-Li-Al alloys, a more uniform and compact corrosion morphology is observed due to the homogeneous distribution of smaller secondary phases throughout the matrix, resulting in the accelerated formation of surface corrosion products [120,244]. Using thin and uniformly distributed second phases can also enhance resistance by creating a protective layer on the surface of alloys, such as the as-extruded Mg-1.21Li-1.12Al-1Y alloy [245]. Purifying Mg-Li-Al alloys to reduce hazardous contaminants and minimize the formation of a strong cathode phase is essential for corrosion resistance. These alloys' corrosion resistance can be strengthened by reducing the volume fraction of the AlLi phase by adding additional alloying elements. Additionally, generating a network phase similar to the $Mg_{17}Al_{12}$ phase at grain boundaries can act as a barrier to prevent corrosion, significantly enhancing the resistance of Mg-Li-Al alloys by including small, uniformly distributed second-phase constituents.

8.3 Surface Film

The corrosion coatings structure is crucial in determining the corrosion rate of magnesium and its alloys. Effective coatings should be thick and stable to prevent the metal substrate from further exposure to air or ions. When magnesium is exposed to air, it spontaneously forms a thin, compact oxide coating consisting of magnesium oxide (MgO) and magnesium hydroxide ($Mg(OH)_2$) with an amorphous structure [246]. This coating typically comprises a amorphous multicellular hydration layer as the innermost layer, with an outermost layer usually ranging from 20 to 40 nanometers thick in damp environments [247]. However, when immersed in water, the surface coating formed on magnesium alloys is often loose and porous, providing inadequate protection for the alloy [246]. The surface film structure and composition of Mg-Li-Al alloys exhibit characteristics influenced by active Li and Al

elements and different crystal structures. Li et al. [93] studied the properties and effectiveness of surface coatings on pure Mg with a hexagonal close-packed (hcp) structure and Mg-14Li alloy with a body-centered cubic (bcc) structure. They observed $Mg(OH)_2$ particles developing on the surfaces of pure Mg, while the surface of Mg-14Li showed needle-like particles with tiny holes. Research suggests that excessive anode overvoltage can lead to the disintegration of both surface layers. In Mg-Li-Al alloys, a thicker oxide coating develops with increasing lithium content, and the presence of dual-phase Mg-Li alloys can further increase corrosion rates, forming a thicker oxide coating [248,249]. The presence of Li in Mg-Li alloys introduces Li-containing compounds into the surface film composition, resulting in a unique multilayer structure. The surface of the Mg-8Li alloy exhibits a four-layer structure when exposed to normal air conditions, with layers consisting of compounds like sodium hydroxide, lithium oxide, magnesium oxide, and lithium hydroxide [250].

Iron and lithium components are readily oxidized in Mg-Li-Al base alloys, forming MgO, Al_2O_3, and Li_2O. A partial hydroxide transformation occurs when these alloys come into contact with water molecules. Thermodynamic studies suggest the substantial presence of $Mg(OH)_2$, Li_2O and Al_2O_3 in the surface coating [251]. Sun et al. [140] observed a four-layer structure in the oxide coating on Mg-Li alloy surfaces after prolonged exposure to air, with the outermost layer primarily composed of lithium compounds like LiOH, Li_2O, and Li_2CO_3. Reference [55] examined the surface and bulk microstructural properties of a new Mg-Li-Al alloy called LATZ9531. He found a six-layer structure of multi-oxide in the surface film, with Li, Mg, and Al being the predominant components. The concentration of Li gradually decreases as one moves inward into the matrix. Alloying elements can significantly influence oxide coatings on metal surfaces, resulting in thinner, denser, and more protective layers [252]. In the LAZ832 alloy, the addition of Yttrium (Y) leads to the growth of numerous tiny, vertically oriented flakes on the surface, enhancing the protective characteristics of the oxide coating and preventing further corrosion of the underlying matrix [109]. The presence of YAl_2 in Mg-Li alloys promotes the Y_2O_3 formation on the surface, improving the adhesive strength between the oxide coating and the substrate material [253]. The protective effectiveness of oxide coatings on metal substrates is often evaluated using the Pilling-Bedworth ratio (PBR) [254]. This ratio, which compares the oxide volume to metal, provides insights into the oxide layer's stress state, integrity, and compactness. A PBR greater than 1 indicates compressive stress in the oxide layer, while values below 1 suggest tensile stress. Larger deviations from unity indicate higher stress levels and a greater likelihood of surface oxide layer rupture [255].

Cain et al. [57] and Xiang et al. [256] attributed the exceptional resistance of corrosion of the Mg-10.95Li-3.29Al-0.19Zr-0.59Y alloy to the production of a stable and protective Li_2CO_3 oxide coating on its surface. Lu et al. [257] conducted a comprehensive study on the chemical composition of surface coatings formed on Mg-Li(-Al-Y-Zr) alloys in air-and water-based solutions. Their analysis revealed that the Mg-Li(-Al-Y-Zr) alloy exhibits a complex, multi-layered surface coating, mainly Li_2CO_3 and $Mg(OH)_2$. The outer layer has a porous structure with a consistent distribution of lithium, while the inner layer consists of a thicker layer formed by combining Li-containing compounds with other substances, enhancing corrosion resistance. Surface films crucial for corrosion resistance often include Li_2CO_3 and $Al_2(CO_3)_3$, which are formed when exposed to carbon dioxide in the air. The dissolution of magnesium, aluminum, and lithium in water generates oxides and hydroxides of these elements. Further studies are needed to fully understand how lithium, aluminum, and rare earth elements affect the stability of these compounds and the corrosion resistance of Mg-Li-Al alloys. Table 5 outlines the factors that influence the corrosion behavior of Mg-Li-Al alloys, detailing the key variables that affect their corrosion resistance.

Table 5: Factors that influence the corrosion behaviour of Mg-Li-Al alloys

Factor		Alloy	Solution	Grain size (μm)	Corrosion rate (mm/a)	References
Grain size	Grain refinement enhances corrosion resistance by densifying grain boundaries and promoting better adhesion of oxide layers.	Mg-13Li-X	Hank's Balanced Salt Solution (HBSS)	4.2	5.830×10^{-7}	[225]
	Large grains reduce the corrosion rate by decreasing the active surface area.	Mg-9Li-3Al-1Ca	0.1 mol/L NaCl	325	5.0	[227]
	Intermediate grain size results in moderate corrosion resistance, balancing between grain boundary density and surface stability.	Mg-9Li-1Zn	0.6 mol/L NaCl	75	0.21	[228]
	Grain refinement by cold-rolling reduces corrosion by increasing grain boundary density and promoting uniform oxide layer formation.	Mg-10Li-1.5Ca	Cold-rolled	59	0.11	[231]
Second phase	Secondary phases, such as Al-Fe and Al-Mn, trigger galvanic corrosion, increasing the overall corrosion rate.	LA83-1.2M	3.5 wt% NaCl	–	–	[242]
	Presence of Li-containing phases results in micro-galvanic corrosion, increasing susceptibility to localized corrosion.	Mg-Li-Al alloys	–	–	–	[245]
	Alloying with Y and Zn reduces micro-galvanic corrosion by modifying the secondary phases and improving the distribution within the matrix.	Mg-6.5Li-0.8Y-0.3Zn	–	–	–	[240]

(Continued)

Table 5 (continued)

Factor		Alloy	Solution	Grain size (μm)	Corrosion rate (mm/a)	References
Surface film	Alloying elements like Al and Y enhance the stability and thickness of oxide coatings, improving corrosion resistance by forming protective layers.	LAZ832	3.5 wt% NaCl	20−30	8.60	[109]
	Increased lithium content leads to thicker and more stable oxide films, reducing overall corrosion rate.	Mg-14Li	–	–	–	[93]
	Effective coatings should be thick and stable. Addition of elements like Al and Y can enhance the composition and protective characteristics of oxide coatings.	Mg-8Li	–	–	–	[250]
	Incorporation of multiple alloying elements results in complex, multilayered oxide films, enhancing overall corrosion resistance by providing a more robust barrier.	LATZ9531	–	–	–	[55]

9 Conclusion

This study presents an in-depth analysis of the Mg-Li-Al alloy system, encompassing a broad range of properties and characteristics. These include structural, electronic, mechanical, and thermodynamic properties, as well as phase stability, corrosion resistance, and potential applications. Using first-principles calculations based on DFT and the quasi-harmonic approximation (QHA), we determined that the Mg-Li-Al phase exhibits higher incompressibility, shear resistance, and stiffness compared to pure Mg-Li, as indicated by its shear modulus, bulk modulus, elastic constants, and Young's modulus. Both phases display brittleness, confirmed by their B/G ratios, Cauchy pressures and Poisson's ratios. The electronic structure analysis revealed metallic behavior for both phases, with Mg-Li-Al showing more covalent bonding characteristics than pure Mg-Li. Mulliken population analysis

emphasized the ionic nature of these phases, with substantial electron transfer from Mg to Al and Li atoms. The bond populations suggest more covalent character in Al-Al bonds in Mg-Li-Al and Mg-Li bonds in pure Mg-Li. The thermodynamic properties, including heat capacity, Debye temperature, enthalpy, free energy, and entropy, were calculated and demonstrated that Mg-Li-Al exhibits a higher Debye temperature and thermal conductivity compared to pure Mg-Li. Both phases follow Debye's law at low temperatures and approach the Dulong−Petit limit at high temperatures, with good agreement between calculated and experimental data for pure Mg-Li. The PHDOS confirmed the dynamic stability of both phases and anisotropic sound velocities indicated elastic anisotropies. To enhance the corrosion resistance of Mg-Li-Al alloys, reducing the AlLi phase through alloying is recommended and creating a network phase similar to Mg-Li-Al as a corrosion barrier. These findings provide valuable insights for developing Mg-Li-Al alloys with improved mechanical and corrosion resistance properties. However, further experimental validation is needed, especially for the Mg-Li-Al phase.

10 Future Recommendations

To further advance the understanding and application of Mg-Li-Al alloys, it is imperative to follow experimental validation of the theoretical predictions. Future research should focus on synthesizing these alloys and conducting detailed characterizations, particularly for the Mg-Li-Al phase. This includes employing high-resolution transmission electron microscopy (HRTEM) and atom probe tomography to analyze the microstructure and distribution of second-phase particles. Such analyses will provide insights into optimizing microstructures for enhanced mechanical and corrosion resistance properties. Introducing alloying elements to reduce the volume fraction of the AlLi phase is a promising direction. Creating a network phase analogous to Mg-Li-Al that acts as a corrosion barrier can significantly improve the longevity of these materials in harsh environments. Long-term corrosion studies in various environmental conditions, including marine and industrial atmospheres, are essential to assess the real-world performance of these alloys. Moreover, developing advanced protective coatings that maintain mechanical integrity while providing effective environmental barriers should be prioritized. Mechanical testing of Mg-Li-Al alloys at elevated temperatures is another crucial area of future research. Investigating the temperature dependence of mechanical properties such as ductility, tensile strength, and creep resistance will provide a more comprehensive understanding of these materials' performance under practical conditions. Further computational studies should explore the effects of various alloying elements, including rare earth metals, to identify potential enhancements in mechanical strength and corrosion resistance. Optimization of processing techniques such as casting, forging, and extrusion is necessary to refine the microstructure and improve the distribution of alloying elements. Simulation studies that mimic real-life applications and loading conditions will help understand the performance of Mg-Li-Al alloys in practical scenarios, such as automotive and aerospace components. Neutron inelastic scattering experiments should be incorporated to gain deeper insights into the phonon dynamics and lattice vibrations of these alloys. This technique will help in understanding the atomic-scale interactions and stability under different environmental conditions. Encouraging interdisciplinary collaboration between materials scientists, mechanical engineers, and corrosion experts will foster innovative solutions addressing multiple aspects of alloy development, leading to more robust and versatile Mg-Li-Al alloys.

Acknowledgement: The authors would like to thank the School of Materials Science and Engineering at North University of China and the Beijing Advanced Innovation Center for Materials Genome

Engineering for their support and resources. Special thanks to colleagues and collaborators for their valuable insights and discussions that contributed to the completion of this review.

Funding Statement: This research did not receive any specific grant from public, commercial, or not-for-profit funding agencies.

Author Contributions: Muhammad Abdullah Khan contributed to the conceptualization, literature search, and initial drafting of the manuscript. Muhammad Usman assisted in gathering relevant studies, critically analyzing the reviewed content, and revising the manuscript for important intellectual content. Yuhong Zhao provided supervision, guided the review process, and contributed to the overall structure and final editing of the manuscript. All authors reviewed the results and approved the final version of the manuscript.

Availability of Data and Materials: No datasets were used or generated during the current study.

Ethics Approval: This study did not involve any human or animal subjects, and therefore, ethical approval was not required.

Conflicts of Interest: The authors declare that they have no conflicts of interest to report regarding the present study.

References

[1] Z. Hao, Y. Ju, and L. Chen, "The use of aluminum and magnesium alloys in automotive lightweight technologies," *J. Mech. Sci. Technol.*, vol. 37, no. 9, pp. 4615–4622, 2023. doi: 10.1007/s12206-023-0712-2.

[2] H. Wang, X. Luo, D. Zhang, C. Qiu, and D. L. Chen, "High-strength extruded magnesium alloys: A critical review," *J. Mater. Sci. Technol.*, vol. 199, pp. 27–52, Nov. 10, 2024. doi: 10.1016/j.jmst.2024.01.089.

[3] K. Sathyanarayana *et al.*, "Metallic lightweight materials: Properties and their applications," *Lightweight Sustain. Comp. Mater.*, vol. 116, no. 1, pp. 47–67, 2023. doi: 10.1016/B978-0-323-95189-0.00003-2.

[4] J. Bai *et al.*, "Applications of magnesium alloys for aerospace: A review," *J. Magnes. Alloys*, vol. 11, no. 10, pp. 3609–3619, Oct. 2023. doi: 10.1016/j.jma.2023.09.015.

[5] Y. Yang, X. Xiong, J. Chen, X. Peng, D. Chen and F. Pan, "Research advances in magnesium and magnesium alloys worldwide in 2020," *J. Magnes. Alloys*, vol. 9, no. 3, pp. 705–747, 2021. doi: 10.1016/j.jma.2021.04.001.

[6] P. Predko *et al.*, "Promising methods for corrosion protection of magnesium alloys in the case of Mg-Al, Mg-Mn-Ce and Mg-Zn-Zr: A recent progress review," *Metals*, vol. 11, no. 7, 2021, Art. no. 1133. doi: 10.3390/met11071133.

[7] I. Bednarczyk, "Characteristics of the microstructure and properties of Mg-Li magnesium alloy after deformation by the Kobo method," *Arch. Metall. Mater.*, pp. 1179–1184, 2022. doi: 10.24425/amm.2022.139718.

[8] L. Wei and Z. Gao, "Recent research advances on corrosion mechanism and protection, and novel coating materials of magnesium alloys: A review," *RSC Adv.*, vol. 13, no. 12, pp. 8427–8463, 2023. doi: 10.1039/D2RA07829E.

[9] R. B. Kumar, M. Y. Ismail, V. S. Vijayarasi, and V. S. Kumar, "Effect of grain refinement on superplastic forming of magnesium alloy AZ31 under three different conditions using rectangular die," *Mater. Today: Proc.*, vol. 22, no. 1–2, pp. 364–369, 2020. doi: 10.1016/j.matpr.2019.06.697.

[10] J. Wei, B. Li, L. Jing, N. Tian, X. Zhao and J. Zhang, "Efficient protection of Mg alloy enabled by combination of a conventional anti-corrosion coating and a superamphiphobic coating," *Chem. Eng. J.*, vol. 390, 2020, Art. no. 124562. doi: 10.1016/j.cej.2020.124562.

[11] A. Bahmani, M. Lotfpour, M. Taghizadeh, and W. Kim, "Corrosion behavior of severely plastically deformed Mg and Mg alloys," *J. Magnes. Alloys*, vol. 10, no. 10, pp. 2607–2648, 2022. doi: 10.1016/j.jma.2022.09.007.

[12] T. Yuan, Y. Wu, Y. Liang, Q. Jiao, Q. Zhang and J. Jiang, "Microstructural control and mechanical properties of a high Li-containing Al-Mg-Li alloy," *Mater. Charact.*, vol. 172, 2021, Art. no. 110895. doi: 10.1016/j.matchar.2021.110895.

[13] H. Ghazanfari *et al.*, "Recent progress in materials used towards corrosion protection of Mg and its alloys," *J. Composit. Compounds*, vol. 2, no. 5, pp. 205–214, 2020. doi: 10.29252/jcc.2.4.5.

[14] W. Fu *et al.*, "Enhancing corrosion resistance of ZK60 magnesium alloys via Ca microalloying: The impact of nanoscale precipitates," *J. Magnes. Alloys*, vol. 11, no. 9, pp. 3214–3230, 2023. doi: 10.1016/j.jma.2022.06.011.

[15] M. G. Acharya and A. N. Shetty, "Influence of media pH on corrosion behavior of AZ31 magnesium alloy in chloride and sulfate media," *Surf. Eng. Appl. Electrochem.*, vol. 57, no. 6, pp. 675–688, 2021. doi: 10.3103/S1068375521060065.

[16] L. Yang, X. Shi, X. Tian, Y. Xue, J. Wang and L. Qi, "Influence of pH value on the microstructure and corrosion behavior of carbon fiber reinforced magnesium matrix composites," *J. Mater. Res. Technol.*, vol. 17, pp. 412–424, 2022. doi: 10.1016/j.jmrt.2022.01.031.

[17] P. Liang *et al.*, "Experimental investigation and thermodynamic calculation of the Al–Mg–Zn system," *Thermochim. Acta*, vol. 314, no. 1–2, pp. 87–110, 1998. doi: 10.1016/S0040-6031(97)00458-9.

[18] C. Guo, S. Shi, H. Dai, J. Yu, and X. Chen, "Corrosion mechanisms of nickel-based alloys in chloride-containing hydrofluoric acid solution," *Eng. Fail. Anal.*, vol. 140, no. 2, 2022, Art. no. 106580. doi: 10.1016/j.engfailanal.2022.106580.

[19] C. Guo, S. Shi, H. Dai, X. Sun, J. Yu and X. Chen, "The deterioration effects of corrosion product deposition on Ni-Cu alloy in hydrofluoric acid vapor phase," *Corros. Sci.*, vol. 219, no. 29–42, 2023, Art. no. 111256. doi: 10.1016/j.corsci.2023.111256.

[20] W. Yang, Z. Liu, and H. Huang, "Galvanic corrosion behavior between AZ91D magnesium alloy and copper in distilled water," *Corros. Sci.*, vol. 188, no. 10, 2021, Art. no. 109562. doi: 10.1016/j.corsci.2021.109562.

[21] N. Wegner and F. Walther, "Assessment of galvanostatic anodic polarization to accelerate the corrosion of the bioresorbable magnesium alloy WE43," *Appl. Sci.*, vol. 11, no. 5, 2021, Art. no. 2128. doi: 10.3390/app11052128.

[22] P. King, "Investigating the role of water quality on the galvanic corrosion of lead in hard drinking water with a focus on NOM", University of Waterloo, Waterloo, ON, Canada, 2020. Accessed: Jun. 05, 2024. [Online]. Available at: http://hdl.handle.net/10012/15913

[23] Y. Li, Z. Shi, X. Chen, and A. Atrens, "Anodic hydrogen evolution on Mg," *J. Magnes. Alloys*, vol. 9, no. 6, pp. 2049–2062, 2021. doi: 10.1016/j.jma.2021.09.002.

[24] P. Volovitch *et al.*, "Synergistic effect of ionic liquid (Il) cation and anion inhibits negative difference effect on mg in water-Il mixtures," *Soc. Sci. Res. Netw.*, vol. 11, no. 9, 2022. doi: 10.2139/ssrn.4145288.

[25] O. I. Velikokhatnyi and P. N. Kumta, "First principles study of the elastic properties of magnesium and iron-based bio-resorbable alloys," *Mater. Sci. Eng. B.*, vol. 230, pp. 20–23, 2018. doi: 10.1016/j.mseb.2017.12.024.

[26] K. S. Williams, J. P. Labukas, V. Rodriguez-Santiago, and J. Andzelm, "First principles modeling of water dissociation on Mg (0001) and development of a Mg surface Pourbaix diagram," *CORROSION*, vol. 71, no. 2, pp. 209–223, 2015. doi: 10.5006/1322.

[27] K. S. Williams, V. Rodriguez-Santiago, and J. W. Andzelm, "Modeling reaction pathways for hydrogen evolution and water dissociation on magnesium," *Electrochim. Acta*, vol. 210, pp. 261–270, 2016. doi: 10.1016/j.electacta.2016.04.128.

[28] K. R. Limmer, K. S. Williams, J. P. Labukas, and J. Andzelm, "First principles modeling of cathodic reaction thermodynamics in dilute magnesium alloys," *CORROSION*, vol. 73, no. 5, pp. 506–517, 2017. doi: 10.5006/2274.

[29] J. A. Yuwono, N. Birbilis, R. Liu, Q. Ou, Q. Bao and N. V. Medhekar, "Aqueous electrochemical activity of the Mg surface: The role of group 14 and 15 microalloying elements," *J. Electrochem. Soc.*, vol. 164, no. 13, 2017, Art. no. C918. doi: 10.1149/2.0071714jes.

[30] A. Sumer and S. Chaudhuri, "A first principles investigation of corrosion chemistry of common elemental impurities in Mg-Al alloys," *CORROSION*, vol. 73, no. 5, pp. 596–604, 2017. doi: 10.5006/2392.

[31] M. McMahon, A. Korjenic, J. Burns, and J. Scully, "Mechanistic insight into Al-Zn, Mg, and Al-Mg-rich primer design for enhanced cathodic prevention on sensitized Al-Mg alloys," *CORROSION*, vol. 79, no. 6, pp. 647–664, 2023. doi: 10.5006/4289.

[32] Q. -Y. Che *et al.*, "Microstructure and mechanical properties of magnesium-lithium alloy prepared by friction stir processing," *Rare Met.*, vol. 40, no. 9, pp. 2552–2559, 2021. doi: 10.1007/s12598-019-01217-2.

[33] S. K. Mishra, V. Manakari, G. Parande, P. R. Matli, and M. Gupta, "Development of ultralight binary Mg-Li alloys: Enhancing damping, ductility, and ultimate compressive strength beyond 2000 MPa," *J. Mater Eng. Perform.*, vol. 32, no. 6, pp. 2723–2734, 2023. doi: 10.1007/s11665-022-07335-w.

[34] Y. Zhu, G. Chen, Y. Zhou, Q. Shi, and M. Zhou, "Achieving synergistic strength-ductility-corrosion optimization in Mg-Li-Al-Zn alloy via cross-pass friction stir processing," *J. Alloys Compounds*, vol. 959, 2023, Art. no. 170581. doi: 10.1016/j.jallcom.2023.170581.

[35] J. Wu *et al.*, "Effect of lithium and aluminum on the mechanical properties, *in vivo* and *in vitro* degradation, and toxicity of multiphase ultrahigh ductility Mg–Li–Al–Zn quaternary alloys for vascular stent application," *ACS Biomater. Sci. Eng.*, vol. 6, no. 4, pp. 1950–1964, 2020. doi: 10.1021/acsbiomaterials.9b01591.

[36] N. Rahulan, S. Gopalan, and S. Kumaran, "Mechanical behavior of Mg-Li-Al alloys," *Mater. Today: Proc.*, vol. 5, no. 9, pp. 17935–17943, 2018. doi: 10.1016/j.matpr.2018.06.123.

[37] N. Mazlan, F. H. Yap, M. Yahya, N. Ali, N. Sazelee and M. Ismail, "Hydrogen storage properties and reaction mechanism of the Mg-Li-Na-Al ternary hydride system," *Mater. Today: Proc.*, vol. 96, pp. 23–29, 2024. doi: 10.1016/j.matpr.2023.08.298.

[38] C. Li *et al.*, "Simultaneously improved mechanical strength and corrosion resistance of Mg-Li-Al alloy by solid solution treatment," *Mater. Lett.*, vol. 301, 2021, Art. no. 130305. doi: 10.1016/j.matlet.2021.130305.

[39] Y. He, C. Peng, Y. Feng, R. Wang, and J. Zhong, "Effects of alloying elements on the microstructure and corrosion behavior of Mg–Li–Al–Y alloys," *J. Alloys Compounds*, vol. 834, no. 6, 2020, Art. no. 154344. doi: 10.1016/j.jallcom.2020.154344.

[40] A. Dhungana, S. K. Yadav, and D. Adhikari, "Thermodynamic and surface properties of Al-Li–Mg liquid alloy," *Physica B: Condensed Matt.*, vol. 598, 2020, Art. no. 412461. doi: 10.1016/j.physb.2020.412461.

[41] G. -L. Song and Z. Xu, "Effect of microstructure evolution on corrosion of different crystal surfaces of AZ31 Mg alloy in a chloride-containing solution," *Corros. Sci.*, vol. 54, pp. 97–105, 2012. doi: 10.1016/j.corsci.2011.09.005.

[42] E. Pugh, "Progress toward understanding the stress corrosion problem," *CORROSION*, vol. 41, no. 9, pp. 517–526, 1985. doi: 10.5006/1.3583022.

[43] G. -L. Song, R. Mishra, and Z. Xu, "Crystallographic orientation and electrochemical activity of AZ31 Mg alloy," *Electrochem. Commun.*, vol. 12, no. 8, pp. 1009–1012, 2010. doi: 10.1016/j.elecom.2010.05.011.

[44] B. -Q. Fu, W. Liu, and Z. -L. Li, "Calculation of the surface energy of hcp-metals with the empirical electron theory," *Appl. Surf. Sci.*, vol. 255, pp. 9348–9357, 2009.

[45] R. Xin, B. Li, L. Li, and Q. Liu, "Influence of texture on corrosion rate of AZ31 Mg alloy in 3.5 wt.% NaCl," *Mater. Des.*, vol. 32, no. 8–9, pp. 4548–4552, 2011. doi: 10.1016/j.matdes.2011.04.031.

[46] D. Bairagi, S. Mandal, M. Roy, M. Paliwal, and S. Mandal, "Enhanced in-vitro degradation resistance and cytocompatibility of a thermomechanically processed novel Mg alloy: Insights into the role of microstructural attributes," *J. Magnes. Alloys*, vol. 12, no. 2, pp. 700–725, Feb. 2024. doi: 10.1016/j.jma.2024.01.022.

[47] V. Verma, S. Singh, and K. Pal, "Exploring the potential of Mg-Zn-Mn-Ca/ZnO composites as a biodegradable alternative for fracture fixation: Microstructural, mechanical, and in-vitro biocompatibility analysis," *Compos. Struct.*, vol. 323, no. 55, 2023, Art. no. 117431. doi: 10.1016/j.compstruct.2023.117431.

[48] B. Feng, X. Shang, T. Xie, T. Ying, and X. Zeng, "Influence of texture on the corrosion behavior of an as-extruded Mg–8Al-0.5In alloy sheet," *J. Mater. Res. Technol.*, vol. 27, pp. 1497–1508, 2023. doi: 10.1016/j.jmrt.2023.10.014.

[49] J. M. Maita *et al.*, "Grain size effect on the mechanical properties of nanocrystalline magnesium aluminate spinel," *Soc. Sci. Res. Netw.*, vol. 251, 2023, Art. no. 118881. doi: 10.1016/j.actamat.2023.118881.

[50] K. Ralston, N. Birbilis, M. Weyland, and C. Hutchinson, "The effect of precipitate size on the yield strength-pitting corrosion correlation in Al–Cu–Mg alloys," *Acta Mater.*, vol. 58, no. 18, pp. 5941–5948, 2010. doi: 10.1016/j.actamat.2010.07.010.

[51] A. Thakur, D. Bandhu, D. Peshwe, Y. Mahajan, K. K. Saxena and S. Eldin, "Appearance of reinforcement, interfacial product, heterogeneous nucleant and grain refiner of $MgAl_2O_4$ in aluminum metal matrix composites," *J. Mater. Res. Technol.*, vol. 26, no. 144, pp. 267–302, 2023. doi: 10.1016/j.jmrt.2023.07.121.

[52] X. Rong *et al.*, "Achieving high mechanical properties and corrosion resistance of Al-Zn-Mg matrix composites via regulating intragranular reinforcements," *J. Mater. Sci. Technol.*, vol. 153, pp. 1–7, 2023. doi: 10.1016/j.jmst.2022.12.066.

[53] M. Vaughan *et al.*, "The effects of severe plastic deformation on the mechanical and corrosion characteristics of a bioresorbable Mg-ZKQX6000 alloy," *Mater. Sci. Eng. C*, vol. 115, 2020, Art. no. 111130. doi: 10.1016/j.msec.2020.111130.

[54] Y. Liu, C. -C. Zhang, X. -Y. Zhang, and Y. -C. Huang, "Understanding grain refinement of Sc addition in a Zr containing Al-Zn-Mg-Cu aluminum alloy from experiments and first-principles," *Intermetallics*, vol. 123, 2020, Art. no. 106823. doi: 10.1016/j.intermet.2020.106823.

[55] S. Tang, "Correlation between microstructure and properties of magnesium-lithium-aluminum alloys," School of Materials Science & Engineering, UNSW Sydney, Australia, 2020. Accessed: Jun. 05, 2024. [Online]. Available: https://unsworks.unsw.edu.au/entities/publication/3990d8c4-6cc4-4e28-a338-326760e3edbc/full

[56] T. Xin, "Phase transformations and mechanical properties of BCC Mg-Li-Al alloys," School of Materials Science & Engineering, UNSW Sydney, Australia, 2021. Accessed: Jun. 05, 2024. [Online]. Available: https://unsworks.unsw.edu.au/entities/publication/e1446fb4-35c0-4872-b33f-d17219eb0fee/full

[57] T. W. Cain and J. P. Labukas, "The development of β phase Mg-Li alloys for ultralight corrosion resistant applications," *npj Mater. Degradat.*, vol. 4, no. 1, 2020, Art. no. 17. doi: 10.1038/s41529-020-0121-2.

[58] X. Yang *et al.*, "Simultaneous improvement of strength, ductility and damping capacity of single β-phase Mg–Li–Al–Zn alloys," *Metals*, vol. 13, no. 1, 2023, Art. no. 159. doi: 10.3390/met13010159.

[59] J. Zhao *et al.*, "Influence of Ca and Zn synergistic alloying on the microstructure, tensile properties and strain hardening of Mg-1Gd alloy," *Mater. Sci. Eng. A.*, vol. 785, no. 15, 2020, Art. no. 139344. doi: 10.1016/j.msea.2020.139344.

[60] S. Riva, K. V. Yusenko, N. P. Lavery, D. J. Jarvis, and S. Brown, "The scandium effect in multicomponent alloys," *Int. Mater. Rev.*, vol. 61, no. 3, pp. 203–228, 2016. doi: 10.1080/09506608.2015.1137692.

[61] Y. Ding, C. Wen, P. Hodgson, and Y. Li, "Effects of alloying elements on the corrosion behavior and biocompatibility of biodegradable magnesium alloys: A review," *J. Mater. Chem. B*, vol. 2, no. 14, pp. 1912–1933, 2014. doi: 10.1039/C3TB21746A.

[62] Y. Chen, Z. Zhu, and J. Zhou, "Study on the strengthening mechanism of rare earth yttrium on magnesium alloys," *Mater. Sci. Eng. A*, vol. 850, no. 1, 2022, Art. no. 143513. doi: 10.1016/j.msea.2022.143513.

[63] S. K. Sharma *et al.*, "Significance of alloying elements on the mechanical characteristics of Mg-based materials for biomedical applications," *Crystals*, vol. 12, no. 8, 2022, Art. no. 1138. doi: 10.3390/cryst12081138.

[64] C. Chakravorty, "Development of ultra-light magnesium-lithium alloys," *Bull. Mater. Sci.*, vol. 17, no. 6, pp. 733–745, 1994. doi: 10.1007/BF02757554.

[65] K. Korgiopoulos and M. Pekguleryuz, "The significant effect of trace yttrium level on the mechanical properties of cast Mg-6Al alloy through a refinement mechanism," *Mater. Sci. Eng. A.*, vol. 775, 2020, Art. no. 138966. doi: 10.1016/j.msea.2020.138966.

[66] Y. K. Li *et al.*, "Tailoring bimodal grain structure of Mg-9Al-1Zn alloy for strength-ductility synergy: Co-regulating effect from coarse Al_2Y and submicron $Mg_{17}Al_{12}$ particles," *J. Magnes. Alloys*, vol. 9, no. 5, pp. 1556–1566, 2021. doi: 10.1016/j.jma.2021.01.008.

[67] H. Hao, X. Liu, C. Fang, and X. Zhang, "Effect of *in-situ* Al2Y particles on the as-cast/as-rolled microstructure and mechanical properties of AZ31 alloy," *Mater. Sci. Eng. A*, vol. 698, pp. 27–35, 2017. doi: 10.1016/j.msea.2017.04.114.

[68] M. Gu, G. Wei, W. Liu, and G. Wu, "Influence of neodymium on microstructure and corrosion behavior of Mg-8Li-3Al-2Zn alloy," vol. 68, pp. 436–443, 2017. doi: 10.1002/maco.201609141.

[69] F. Czerwinski, "Cerium in aluminum alloys," *Mater. Corrosion*, vol. 55, no. 4, pp. 24–72, 2020. doi: 10.1007/s10853-019-03892-z.

[70] P. Dinesh, S. KumareshBabu, and S. Natarajan, "Effect of lanthanum addition on grain refinement and mechanical properties of Mg–9Li–3Al alloy," *Met. Mater. Int.*, vol. 27, no. 10, pp. 3993–4001, 2021. doi: 10.1007/s12540-020-00776-9.

[71] Y. Chen *et al.*, "CALPHAD-guided design of Mg-Y-Al alloy with improved strength and ductility via regulating the LPSO phase," *Acta Mater.*, vol. 263, no. 4, 2024, Art. no. 119521. doi: 10.1016/j.actamat.2023.119521.

[72] X. Zhang *et al.*, "Improving the mechanical properties of duplex Mg-Li-Zn alloy by mixed rolling processing," *Mater. Today Commun.*, vol. 31, no. 3, 2022, Art. no. 103538. doi: 10.1016/j.mtcomm.2022.103538.

[73] X. Geng, L. Hong, J. Jiang, and X. Zhang, "Effects of solution temperature and Nd addition on microstructure and mechanical properties of Mg-12Gd-2Zn-x Nd-0.4 Zr alloys," *J. Mater. Eng. Perform.*, vol. 33, no. 18, pp. 9802–9812, 2024. doi: 10.1007/s11665-023-08628-4.

[74] P. Metalnikov, G. Ben-Hamu, and K. Shin, "Relation between Zn additions, microstructure and corrosion behavior of new wrought Mg-5Al alloys," *Met. Mater. Int.*, vol. 27, no. 6, pp. 1493–1505, 2021. doi: 10.1007/s12540-019-00529-3.

[75] Y. -G. Jung *et al.*, "Effect of Ca addition on the microstructure and mechanical properties of heat-treated Mg-6.0 Zn-1.2 Y-0.7 Zr alloy," *J. Magnes. Alloys*, vol. 9, no. 5, pp. 1619–1631, 2021. doi: 10.1016/j.jma.2021.01.010.

[76] M. X. Li *et al.*, "Tailoring the microstructure and enhancing the corrosion resistance of extruded dilute Mg-0.6 Al-0.5 Mn-0.25 Ca alloy by adding trace Ce," *Corros. Sci.*, vol. 207, 2022, Art. no. 110605. doi: 10.1016/j.corsci.2022.110605.

[77] T. Fu *et al.*, "Achieving high strength-ductility synergy in dilute Mg-Al-Ca alloy by trace Ce addition," *J. Alloys Compounds*, vol. 917, no. 1, 2022, Art. no. 165407. doi: 10.1016/j.jallcom.2022.165407.

[78] X. Wang, C. Chen, and M. Zhang, "Effect of Cu addition and heat treatment on the microstructure and microwear of selective laser melted Mg–Al–Zn alloy," *Appl. Phys. A*, vol. 126, no. 9, pp. 1–19, 2020. doi: 10.1007/s00339-020-03917-4.

[79] N. Fang, H. Wang, Z. Wei, C. Zou, J. Chen and T. Chang, "Microstructural characteristics and mechanical performances of Al–Si–Cu–Mg-(Ge) alloys prepared under 5GPa-level pressure," *Mater. Sci. Eng. A*, vol. 876, no. 4, 2023, Art. no. 145118. doi: 10.1016/j.msea.2023.145118.

[80] P. Gogola, Z. Gabalcová, M. Kusý, and H. Suchánek, "The effect of Sn addition on Zn-Al-Mg alloy: Part I: Microstructure and phase composition," *Materials*, vol. 14, no. 18, 2021, Art. no. 5404. doi: 10.3390/ma14185404.

[81] H. Cao *et al.*, "Experimental investigation and thermodynamic modelling of the Mg-Al-rich region of the Mg–Al–Sr," *Int. J. Mater. Res.*, vol. 97, pp. 422–428, 2022. doi: 10.1515/ijmr-2006-0070.

[82] T. Mandal, S. Dasgupta, A. Barui, and S. Kundu, "Effect of strontium on microstructure, mechanical, and biological responses of Mg–Al–Zn–Sr alloys," *Mater. Sci. Technol.*, vol. 38, no. 14, pp. 1134–1150, 2022. doi: 10.1080/02670836.2022.2072071.

[83] H. Yaykaşlı and M. Göğebakan, "Effect of boron addition on the microstructure, thermal, and mechanical properties of Al-5% Mg-2% Ti alloy," *Metallogr., Microstruct., Analy.*, vol. 13, pp. 296–306, 2024.

[84] Y-K. Taninouchi, T. Yamaguchi, T. H. Okabe, and H. Nakano, "Solubility of chromium in liquid magnesium," *Metall. Mater. Trans. B*, vol. 53, no. 3, pp. 1851–1857, 2022. doi: 10.1007/s11663-022-02494-6.

[85] T. B. H. Nguyen, H. -T. Van, T. N. H. Tran, T. T. Nguyen, and T. K. Hoang, "Insight into chromium adsorption from contaminated soil using Mg/Al LDH-zeolite," *Heliyon*, vol. 10, no. 10, 2024, Art. no. e31084. doi: 10.1016/j.heliyon.2024.e31084.
[86] T. Chen *et al.*, "Effect of Mn addition on melt purification and Fe tolerance in Mg alloys," *JOM*, vol. 73, no. 3, pp. 892–902, 2021. doi: 10.1007/s11837-020-04550-5.
[87] W. Liu *et al.*, "Microstructure and mechanical properties of extruded Mg-6Al-2X (X = Cu/Ni/Fe) alloy used degradable bridge plugs," *Adv. Compos. Hybrid Mater.*, vol. 6, no. 5, p. 181, 2023. doi: 10.1007/s42114-023-00753-x.
[88] N. Loukil, "Alloying elements of magnesium alloys: A literature review," *Magnes. Alloys Struct. Propert.*, vol. 17, pp. 58–78, 2021. doi: 10.5772/intechopen.96232.
[89] M. Yamasaki, Z. Shi, A. Atrens, A. Furukawa, and Y. Kawamura, "Influence of crystallographic orientation and Al alloying on the corrosion behavior of extruded α-Mg/LPSO two-phase Mg-Zn-Y alloys with multimodal microstructure," *Corros. Sci.*, vol. 200, no. 32, 2022, Art. no. 110237. doi: 10.1016/j.corsci.2022.110237.
[90] A. Atrens *et al.*, "Review of Mg alloy corrosion rates," *J. Magnes. Alloys*, vol. 8, no. 4, pp. 989–998, 2020. doi: 10.1016/j.jma.2020.08.002.
[91] Z. Zeng *et al.*, "Corrosion resistant and high-strength dual-phase Mg-Li-Al-Zn alloy by friction stir processing," *Commun. Mater.*, vol. 3, no. 1, 2022, Art. no. 18. doi: 10.1038/s43246-022-00245-3.
[92] F. Cao, J. Zhang, K. K. Li, and G. Song, "Influence of heat treatment on corrosion behavior of hot rolled Mg5Gd alloys," *Trans. Nonferrous Met. Soc. China*, vol. 31, no. 4, pp. 939–951, 2021. doi: 10.1016/S1003-6326(21)65551-6.
[93] C. Li, Y. He, and H. Huang, "Effect of lithium content on the mechanical and corrosion behaviors of HCP binary Mg-Li alloys," *J. Magnes. Alloys*, vol. 9, no. 2, pp. 569–580, 2021. doi: 10.1016/j.jma.2020.02.022.
[94] A. A. Abildina *et al.*, "Corrosion behavior of magnesium in aqueous sulfate-containing electrolytes," *J. Magnes. Alloys*, vol. 11, no. 6, pp. 2125–2141, 2023. doi: 10.1016/j.jma.2023.06.001.
[95] B. Wang, J. Hou, J. Luan, D. Xu, H. Sun and J. Sun, "The corrosion behaviors of an as-rolled Mg-8Li (in wt.%) alloy in two differently concentrated NaCl solutions," *Coatings*, vol. 12, no. 3, 2022, Art. no. 406. doi: 10.3390/coatings12030406.
[96] A. Dobkowska *et al.*, "Microstructure and corrosion resistance of a duplex structured Mg–7.5Li–3Al–1Zn," *J. Magnes. Alloys*, vol. 9, no. 2, pp. 467–477, 2021. doi: 10.1016/j.jma.2020.07.007.
[97] J. Feng, H. Zhang, L. Zhang, G. Zou, J. Wang and Q. Peng, "Microstructure and corrosion properties for ultrahigh-pressure Mg-Li alloys," *Corros. Sci.*, vol. 206, 2022, Art. no. 110519. doi: 10.1016/j.corsci.2022.110519.
[98] Y. Yan *et al.*, "On the *in-situ* aqueous stability of an Mg-Li-(Al-Y-Zr) alloy: Role of Li," *Corros. Sci.*, vol. 164, 2020, Art. no. 108342. doi: 10.1016/j.corsci.2019.108342.
[99] Y. Zhu *et al.*, "Microstructural evolution and its influence on mechanical and corrosion behaviors in a high-Al/Zn containing duplex Mg-Li alloy after friction stir processing," *J. Mater. Sci. Technol.*, vol. 184, 2024, Art. no. 245–255. doi: 10.1016/j.jmst.2023.10.019.
[100] C. Zhang *et al.*, "Effect of microalloyed Ca on the microstructure and corrosion behavior of extruded Mg alloy AZ31," *J. Alloys Compounds*, vol. 823, 2020, Art. no. 153844. doi: 10.1016/j.jallcom.2020.153844.
[101] J. Xie *et al.*, "Towards developing Mg alloys with simultaneously improved strength and corrosion resistance via RE alloying," *J. Magnes. Alloys*, vol. 9, no. 1, pp. 41–56, 2021. doi: 10.1016/j.jma.2020.08.016.
[102] V. Kumar, R. Shekhar, and K. Balani, "Corrosion behavior of novel Mg-9Li-7Al-1Sn and Mg-9Li-5Al-3Sn-1Zn alloys in NaCl aqueous solution," *J. Mater. Eng. Perform.*, vol. 24, no. 10, pp. 4060–4070, 2015. doi: 10.1007/s11665-015-1687-7.
[103] C. Okafor, A. Datye, S. Zhang, U. D. Schwarz, Y. Cai and N. Munroe, "Development and biomaterial characterization of Mg-Li-Zn-Ca alloys," *Soc. Sci. Res. Netw.*, vol. 33, 2022, Art. no. 104999.
[104] Y. Xiong, L. Deng, and P. Wei, "Effect of Ca content on the mechanical properties and corrosion behaviors of extruded Mg–7Li–3Al alloys," *Metals*, vol. 9, no. 11, 2019, Art. no. 1212. doi: 10.3390/met9111212.

[105] C. -Q Li, Z. -P Tong, Y. -B He, H. -P Huang, D. Yong and P. Zhang, "Comparison on corrosion resistance and surface film of pure Mg and Mg−14Li alloy," *Trans. Nonferrous Met. Soc. China*, vol. 30, no. 9, pp. 2413–2423, 2020. doi: 10.1016/S1003-6326(20)65388-2.

[106] Y. Dai *et al.*, "Improved corrosion resistance in AZ61 magnesium alloys induced by impurity reduction," *Acta Metallurgica Sin.*, vol. 33, no. 2, pp. 225–232, 2020. doi: 10.1007/s40195-019-00914-2.

[107] G. Tian *et al.*, "Designing strong and stiff HCP and BCC Mg alloy structures by templating hard faceted phase using Sn and RE elements," *J. Alloys Compounds*, vol. 976, no. 3, 2024, Art. no. 173291. doi: 10.1016/j.jallcom.2023.173291.

[108] W. Weng, A. Biesiekierski, Y. Li, M. Dargusch, and C. Wen, "A review of the physiological impact of rare earth elements and their uses in biomedical Mg alloys," *Acta Biomater.*, vol. 130, no. 3, pp. 80–97, 2021. doi: 10.1016/j.actbio.2021.06.004.

[109] M. Gu, G. Wei, J. Zhao, W. Liu, and G. Wu, "Influence of yttrium addition on the corrosion behavior of as-cast Mg–8Li–3Al–2Zn alloy," *Mater. Sci. Technol.*, vol. 33, no. 7, pp. 864–869, 2017. doi: 10.1080/02670836.2016.1244140.

[110] H. -W. Chang, D. Qiu, J. A. Taylor, M. A. Easton, and M. -X. Zhang, "The role of Al_2Y in grain refinement in Mg–Al–Y alloy system," *J. Magnes. Alloys*, vol. 1, no. 2, pp. 115–121, 2013. doi: 10.1016/j.jma.2013.07.006.

[111] Y. Sun, R. Wang, C. Peng, and Y. Feng, "Effects of Sn and Y on the microstructure, texture, and mechanical properties of as-extruded Mg-5Li-3Al-2Zn alloy," *Mater. Sci. Eng. A.*, vol. 733, pp. 429–439, 2018. doi: 10.1016/j.msea.2018.05.030.

[112] Z. Liu, S. Yang, Y. Li, M. Ma, and S. Han, "Improved electrochemical kinetic performances of La-Mg-Ni-based hydrogen storage alloys with lanthanum partially substituted by yttrium," *J. Rare Earths*, vol. 33, pp. 397–402, 2015. doi: 10.1016/S1002-0721(14)60432-4.

[113] D. Malavekar, V. Magdum, S. Khot, J. Kim, and C. Lokhande, "Doping of rare earth elements: Towards enhancing the electrochemical performance of pseudocapacitive materials," *J. Alloys Compounds*, vol. 960, no. 313, 2023, Art. no. 170601. doi: 10.1016/j.jallcom.2023.170601.

[114] F. Cao, Z. Shi, G. -L. Song, M. Liu, M. S. Dargusch and A. Atrens, "Influence of hot rolling on the corrosion behavior of several Mg-X alloys," *Corros. Sci.*, vol. 90, pp. 176–191, 2015. doi: 10.1016/j.corsci.2014.10.012.

[115] Z. Zhao, Z. Sun, W. Liang, Y. Wang, and L. Bian, "Influence of Al and Si additions on the microstructure and mechanical properties of Mg-4Li alloys," *Mater. Sci. Eng. A*, vol. 702, pp. 206–217, 2017. doi: 10.1016/j.msea.2017.06.077.

[116] H. -M. Yang, N. -Y. Zhang, N. Liu, W. -D. Xie, and X. Peng, "Microstructure, mechanical properties, and corrosion resistance of Mg–9Li–3Al–1.6Y alloy," *Rare Met.*, vol. 35, no. 5, pp. 374–379, 2016. doi: 10.1007/s12598-014-0227-1.

[117] X. Lei, R. Wang, C. Peng, Y. Feng, and Y. Sun, "Effect of hot extrusion on the microstructure, mechanical properties, and corrosion behavior of Mg–11Li–3Al–2Zn–1.5Nd–0.2Zr alloy," *Trans. Indian Ins. Met.*, vol. 72, no. 10, pp. 2893–2899, 2019. doi: 10.1007/s12666-019-01765-2.

[118] C. Ma, X. Ma, X. Pei, Y. Xu, P. Peng and N. Wang, "Effect of rolling reduction on the microstructure and mechanical properties of hot-rolled Mg-Li-Al-Ca alloys," *Mater. Today Commun.*, vol. 37, 2023, Art. no. 107469. doi: 10.1016/j.mtcomm.2023.107469.

[119] G. Ma, G. Wu, W. Shi, S. Xiang, Q. Chen and X. Mao, "Effect of cold rolling on the corrosion behavior of Ta-4W alloy in sulphuric acid," *Corros. Sci.*, vol. 176, 2020, Art. no. 108924. doi: 10.1016/j.corsci.2020.108924.

[120] S. -S. Lim *et al.*, "Study on rolling defects of Al-Mg alloys with high Mg content in normal rolling and cross-rolling processes," *Materials*, vol. 16, no. 18, 2023, Art. no. 6260. doi: 10.3390/ma16186260.

[121] X. Peng, W. Liu, G. Wu, H. Ji, and W. Ding, "Plastic deformation and heat treatment of Mg-Li alloys: A review," *J. Mater. Sci. Technol.*, vol. 99, pp. 193–206, 2022. doi: 10.1016/j.jmst.2021.04.072.

[122] Z. -S. Wei *et al.*, "Exfoliation corrosion of as-extruded Mg–1Li–1Ca: The influence of the superficial layer," *Acta Metall. Sin.*, vol. 37, no. 8, pp. 1339–1353, 2024. doi: 10.1007/s40195-024-01708-x.

[123] Q. Sun, M. Yang, Y. Jiang, L. Lei, and Y. Zhang, "Achieving excellent corrosion resistance properties of 7075 Al alloy via ultrasonic surface rolling treatment," *J. Alloys Compounds*, vol. 911, 2022, Art. no. 165009. doi: 10.1016/j.jallcom.2022.165009.
[124] S. Sarkar, S. Mukherjee, C. S. Kumar, and A. Nath, "Effects of heat treatment on microstructure, mechanical and corrosion properties of 15-5 PH stainless steel parts built by selective laser melting process," *J. Manufact. Process.*, vol. 50, pp. 279–294, 2020.
[125] D. Wang, P. Fu, L. Peng, Y. Wang, and W. Ding, "A study of microstructure, mechanical behavior and strengthening mechanism in the Mg-10Gd-0.2 Zn-(Y)-0.4 Zr alloy," *Mater. Sci. Eng. A.*, vol. 793, 2020, Art. no. 139881.
[126] J. Wang, Y. Zou, C. Dang, Z. Wan, J. Wang and F. Pan, "Research progress and the prospect of damping magnesium alloys," *Materials*, vol. 17, no. 6, 2024, Art. no. 1285. doi: 10.3390/ma17061285.
[127] Z. Ma *et al.*, "Hot deformation behavior and microstructural evolution for dual-phase Mg-9Li–3Al alloys," *J. Mater. Res. Technol.*, vol. 19, no. 1, pp. 3536–3545, 2022. doi: 10.1016/j.jmrt.2022.06.047.
[128] L. Ma. *et al.*, "Effect of rolling reduction and annealing process on microstructure and corrosion behavior of LZ91 alloy sheet," *Trans. Nonferrous Met. Soc. China*, vol. 30, pp. 1816–1825, 2020. doi: 10.1016/S1003-6326(20)65341-9.
[129] F. Guo, L. Liu, Y. Ma, L. Jiang, D. Zhang and F. Pan, "Mechanism of phase refinement and its effect on mechanical properties of a severely deformed dual-phase Mg-Li alloy during annealing," *Mater. Sci. Eng. A.*, vol. 772, 2020, Art. no. 138792.
[130] A. Dobkowska *et al.*, "Corrosion behavior of fine-grained Mg-7.5 Li-3Al-1Zn fabricated by extrusion with a forward-backward rotating die (KoBo)," *J. Magnes. Alloys*, vol. 10, no. 3, pp. 811–820, 2022. doi: 10.1016/j.jma.2021.08.020.
[131] A. Dobkowska *et al.*, "Influence of bimodal grain size distribution on the corrosion resistance of Mg–4Li–3Al–1Zn (LAZ431)," *J. Mater. Res. Technol.*, vol. 13, pp. 346–358, 2021. doi: 10.1016/j.jmrt.2021.04.078.
[132] J. Song, J. She, D. Chen, and F. Pan, "Latest research advances on magnesium and magnesium alloys worldwide," *J. Magnes. Alloys*, vol. 8, no. 1, pp. 1–41, 2020. doi: 10.1016/j.jma.2020.02.003.
[133] S. K. Sharma *et al.*, "Advancements in the additive manufacturing of magnesium and aluminum alloys through laser-based approach," *Materials*, vol. 15, no. 22, 2022, Art. no. 8122. doi: 10.3390/ma15228122.
[134] H. M. Ahmed, H. A. Ahmed, M. Hefni, and E. B. Moustafa, "Effect of grain refinement on the dynamic, mechanical properties, and corrosion behaviour of Al-Mg alloy," *Metals*, vol. 11, no. 11, 2021, Art. no. 1825. doi: 10.3390/met11111825.
[135] P. Minárik, R. Král, and M. Janeček, "Effect of ECAP processing on corrosion resistance of AE21 and AE42 magnesium alloys," *Appl. Surf. Sci.*, vol. 281, pp. 44–48, 2013. doi: 10.1016/j.apsusc.2012.12.096.
[136] B. -C. Liu, S. Zhang, H. -W. Xiong, W. -H. Dai, and Y. Ma, "Effect of Al content on the corrosion behavior of extruded dilute Mg–Al–Ca–Mn alloy," *Acta Metall. Sin.*, vol. 36, no. 1, pp. 77–90, 2023.
[137] T. -C. Chang, J. -Y. Wang, C. -L. Chu, and S. Lee, "Mechanical properties and microstructures of various Mg-Li alloys," *Mater. Lett.*, vol. 60, no. 27, pp. 3272–3276, 2006. doi: 10.1016/j.matlet.2006.03.052.
[138] Z. Guo *et al.*, "High-strength β-phase magnesium-lithium alloy prepared by multidirectional rolling," *Materials*, vol. 16, no. 8, 2023, Art. no. 3227. doi: 10.3390/ma16083227.
[139] C. Li, D. Xu, Z. Zhang, and E. Han, "Influence of the lithium content on the negative difference effect of Mg-Li alloys," *J. Mater. Sci. Technol.*, vol. 57, pp. 138–145, 2020. doi: 10.1016/j.jmst.2020.03.046.
[140] Y. Sun, R. Wang, C. Peng, and Z. Cai, "Microstructure and corrosion behavior of as-extruded Mg-xLi-3Al-2Zn-0.2 Zr alloys (x = 5, 8, 11 wt.%)," *Corros. Sci.*, vol. 167, 2020, Art. no. 108487. doi: 10.1016/j.corsci.2020.108487.
[141] G. Tian *et al.*, "Improving corrosion resistance of Mg-Li alloys by Sn microalloying," *J. Mater. Res. Technol.*, vol. 26, no. 3, pp. 199–217, 2023. doi: 10.1016/j.jmrt.2023.07.205.
[142] J. Wang *et al.*, "First-principle study of the basal-plane stacking fault energies of ternary Mg alloys," *J. Mater. Sci.*, vol. 57, pp. 18417–18436, 2022.

[143] Y. Tang, W. Jia, X. Liu, Q. Le, and Y. Zhang, "Fabrication of high strength α, $\alpha+\beta$, β phase containing Mg-Li alloys with 0.2%Y by extruding and annealing process," *Mater. Sci. Eng. A*, vol. 675, pp. 55–64, 2016.

[144] X. Liu, J. Xue, and S. Liu, "Discharge and corrosion behaviors of the α-Mg and β-Li based Mg alloys for Mg-air batteries at different current densities," *Mater. Des.*, vol. 160, pp. 138–146, 2018. doi: 10.1016/J.MATDES.2018.09.011.

[145] O. Pavlic *et al.*, "Design of Mg alloys: The effects of Li concentration on the structure and elastic properties in the Mg-Li binary system by first principles calculations," *J. Alloys Compounds*, vol. 691, pp. 15–25, 2017. doi: 10.1016/j.jallcom.2016.08.217.

[146] F. Xu, L. Luo, L. Xiong, and Y. Liu, "Microstructure and corrosion behavior of ALD Al_2O_3 film on AZ31 magnesium alloy with different surface roughness," *J. Magnes. Alloys*, vol. 8, pp. 480–492, 2020.

[147] T. O. Olugbade, B. O. Omiyale, and O. Ojo, "Corrosion, corrosion fatigue, and protection of magnesium alloys: Mechanisms, measurements, and mitigation," *J. Mater. Eng. Perform.*, vol. 31, no. 3, pp. 1707–1727, 2022. doi: 10.1007/s11665-021-06355-2.

[148] M. Ramli, M. Romzi, and J. Alias, "Effect of surface condition on the corrosion behavior of AZ31 magnesium alloy," *Mater. Today: Proc.*, vol. 48, no. 5, pp. 747–752, 2022. doi: 10.1016/j.matpr.2021.02.213.

[149] M. Wischhusen, C. Glover, P. K. Liaw, J. R. Scully, and S. Agnew, "Pitting corrosion susceptibility of microstructural features in a compositionally complex ferritic steel as a function of titanium concentration," *CORROSION*, vol. 78, pp. 280–292, 2022.

[150] G. -L. Song and A. Atrens, "Recently deepened insights regarding Mg corrosion and advanced engineering applications of Mg alloys," *J. Magnes. Alloys*, vol. 11, no. 11, pp. 3948–3991, Nov. 2023. doi: 10.1016/j.jma.2023.08.012.

[151] O. B. Istanbullu and G. Akdogan, "A simulation study of galvanic corrosion potential on the surface of implantable biometallic couples," *J. Bio- Tribo-Corrosion*, vol. 7, no. 1, 2021, Art. no. 25. doi: 10.1007/s40735-020-00462-8.

[152] V. Torres, R. Mayen-Mondragon, and J. Genesca, "Assessment of the galvanic corrosion of bi-metallic couple 7075-T6-aluminum alloy/microalloyed dual-phase steel," *Mater. Corros.*, vol. 73, no. 6, pp. 940–949, 2022. doi: 10.1002/maco.202112934.

[153] D. -H. Xia *et al.*, "Electrochemical measurements used for assessment of corrosion and protection of metallic materials in the field: A critical review," *J. Mater. Sci. Technol.*, vol. 112, no. 2, 2022, Art. no. 151–183. doi: 10.1016/j.jmst.2021.11.004.

[154] J. Jiang, X. Geng, and X. Zhang, "Stress corrosion cracking of magnesium alloys: A review," *J. Magnes. Alloys*, vol. 11, no. 6, pp. 1906–1930, Jun. 2023. doi: 10.1016/j.jma.2023.05.011.

[155] M. López Freixes *et al.*, "Revisiting stress-corrosion cracking and hydrogen embrittlement in 7xxx-Al alloys at the near-atomic-scale," *Nat. Commun.*, vol. 13, 2022, Art. no. 4290. doi: 10.1038/s41467-022-31964-3.

[156] M. Safyari, M. Moshtaghi, S. Kuramoto, and T. Hojo, "Influence of microstructure-driven hydrogen distribution on environmental hydrogen embrittlement of an Al–Cu–Mg alloy," *Int. J. Hydrogen Energy*, vol. 46, no. 75, pp. 37502–37508, 2021. doi: 10.1016/j.ijhydene.2021.09.013.

[157] J. Song, J. Chen, X. Xiong, X. Peng, D. Chen and F. Pan, "Research advances of magnesium and magnesium alloys worldwide in 2021," *J. Magnes. Alloys*, vol. 10, no. 4, pp. 863–898, 2022. doi: 10.1016/j.jma.2022.04.001.

[158] M. Shahabi-Navid *et al.*, "On the early stages of localised atmospheric corrosion of magnesium-aluminium alloys," *Sci. Rep.*, vol. 10, no. 1, 2020, Art. no. 20972. doi: 10.1038/s41598-020-78030-w.

[159] Z. Yin *et al.*, "Effects of surface micro-galvanic corrosion and corrosive film on the corrosion resistance of AZ91-xNd alloys," *Appl. Surf. Sci.*, vol. 536, 2021, Art. no. 147761.

[160] X. Liu *et al.*, "Research progress in the environmental application of magnesium hydroxide nanomaterials," *Surf. Interfaces*, vol. 21, 2020, Art. no. 100701.

[161] J. Oh, Y. Lee, and J. Yoh, "On the oxidation kinetics of aging magnesium particles," *Combust. Flame*, vol. 249, 2023, Art. no. 112597. doi: 10.1016/j.combustflame.2022.112597.

[162] H. Wang, Y. Song, D. Shan, and E. Han, "Effects of corrosive media on the localized corrosion forms of Mg-3Zn alloy," *Corros. Commun.*, vol. 2, pp. 24–32, 2021. doi: 10.1016/j.corcom.2021.08.002.

[163] Z. Chen, H. Li, X. Liang, M. -C. Zhao, K. Zhang and A. Atrens, "*In-situ* observation on filiform corrosion propagation and its dependence on Zr distribution in Mg alloy WE43," *J. Magnes. Alloys*, vol. 11, no. 11, pp. 4282–4300, 2023. doi: 10.1016/j.jma.2022.09.033.

[164] Q. Jin, L. Zhi, D. -Q. Yi, and W. Bin, "Diversity of intergranular corrosion and stress corrosion cracking for 5083 Al alloy with different grain sizes," *Trans. Nonferrous Met. Soc. China*, vol. 32, pp. 765–777, 2022. doi: 10.1016/S1003-6326(22)65831-X.

[165] A. Cristoforetti, S. Rossi, F. Deflorian, and M. Fedel, "Exploring the role of passivating conversion coatings in enhancing the durability of organic-coated steel against filiform corrosion using an electrochemical simulated approach," *Prog. Org. Coat.*, vol. 189, 2024, Art. no. 108357. doi: 10.1016/j.porgcoat.2024.108357.

[166] Z. Li, Z. Peng, K. Qi, H. Li, Y. Qiu and X. Guo, "Microstructure and corrosion of cast magnesium alloy ZK60 in NaCl solution," *Materials*, vol. 13, no. 17, 2020, Art. no. 3833. doi: 10.3390/ma13173833.

[167] Y. Sun, R. Wang, C. Peng, and X. Wang, "Microstructure and corrosion behavior of as-homogenized Mg-xLi-3Al-2Zn-0.2Zr alloys (x = 5, 8, 11 wt%)," *Mater. Charact.*, vol. 159, 2020, Art. no. 110031. doi: 10.1016/j.matchar.2019.110031.

[168] I. Nakatsugawa and Y. Chino, "Effect of area ratio on the galvanic corrosion of AZX611 magnesium alloy/A6N01 aluminum alloy joint," *Eng. Mater. App.*, vol. 62, no. 12, pp. 1764–1770, 2021. doi: 10.2320/matertrans.MT-L2021011.

[169] J. Xie *et al.*, "Corrosion mechanism of Mg alloys involving elongated long-period stacking ordered phase and intragranular lamellar structure," *J. Mater. Sci. Technol.*, vol. 151, pp. 190–203, 2023. doi: 10.1016/j.jmst.2023.01.005.

[170] L. Wang, J. Jiang, H. Liu, B. Saleh, and A. Ma, "Microstructure characterization and corrosion behavior of Mg–Y–Zn alloys with different long period stacking ordered structures," *J. Magnes. Alloys*, vol. 8, no. 4, pp. 1208–1220, 2020. doi: 10.1016/j.jma.2019.12.009.

[171] J. Tian, G. Yang, Z. Lei, J. Huang, Z. Zhang and J. Xie, "Effect of long period stacking ordered structure on the biocorrosion resistance and osteogenesis ability of Mg–Zn–Y–Mn alloys," *Mater. Lett.*, vol. 347, no. 16, 2023, Art. no. 134606. doi: 10.1016/j.matlet.2023.134606.

[172] C. Dai *et al.*, "Tailoring the microstructural characteristic and improving the corrosion rate of Mg-Gd-Ni alloy by heat treatment with different volume fraction of LPSO phase," *Corros. Sci.*, vol. 210, 2023, Art. no. 110806.

[173] M. S. Geshani, P. M. Kalayeh, A. H. Asadi, H. Mirzadeh, M. Malekan and M. Emamy, "A review of Mg alloys containing long-period stacking ordered (LPSO) structures with insight into the application of friction stir processing," *J. Mater. Res. Technol.*, vol. 24, no. 3, pp. 4945–4966, 2023. doi: 10.1016/j.jmrt.2023.04.105.

[174] M. Legrée, J. -L. Bobet, F. Mauvy, and J. Sabatier, "Modeling hydrolysis kinetics of dual phase α-Mg/LPSO alloys," *Int. J. Hydrogen Energy*, vol. 47, no. 55, 2022, Art. no. 23084–23093. doi: 10.1016/j.ijhydene.2022.05.001.

[175] F. Z. Akbarzadeh, E. R. Ghomi, and S. Ramakrishna, "Improving the corrosion behavior of magnesium alloys with a focus on AZ91 Mg alloy intended for biomedical application by microstructure modification and coating," *Proc. Instit. Mech. Eng., Part H: J. Eng. Med.*, vol. 236, no. 8, pp. 1188–1208, 2022. doi: 10.1177/09544119221105705.

[176] D. Dubey *et al.*, "Comparative study on the stress corrosion cracking susceptibility of AZ80 and AZ31 magnesium alloys," *Mater. Sci. Eng. A*, vol. 792, 2020, Art. no. 139793.

[177] Y. Li, Y. Liu, and J. Yang, "First principle calculations and mechanical properties of the intermetallic compounds in a laser welded steel/aluminum joint," *Opt. Las. Technol.*, vol. 122, 2020, Art. no.105875.

[178] F. Wang, J. Li, C. Shi, E. Liu, C. He and N. Zhao, "Comparison of electronic structures and mechanical properties of $MgAlB_4$, AlB_2 and MgB_2 using first-principles calculations," *Ceram. Int.*, vol. 46, pp. 12548–12558, 2020.

[179] Z. Huang, Y. Zhao, H. Hou, and P. Han, "Electronic structural, elastic properties, and thermodynamics of $Mg_{17}Al_{12}$, Mg_2Si, and Al_2Y phases from first-principles calculations," *Physica B: Condensed Matt.*, vol. 407, pp. 1075–1081, 2012.

[180] D. Zhou, J. Liu, S. Xu, and P. Peng, "Thermal stability and elastic properties of Mg_3Sb_2 and Mg_3Bi_2 phases from first-principles calculations," *Physica B: Condensed Matt.*, vol. 405, no. 13, pp. 2863–2868, 2010. doi: 10.1016/j.physb.2010.04.013.

[181] H. Zhang, S. Shang, Y. Wang, A. Saengdeejing, L. Chen and Z. K. Liu, "First-principles calculations of the elastic, phonon, and thermodynamic properties of $Al_{12}Mg_{17}$," *Acta Materialia*, vol. 58, no. 11, pp. 4012–4018, 2010. doi: 10.1016/j.actamat.2010.03.020.

[182] S. Ganeshan, S. Shang, H. Zhang, Y. Wang, and Z. -K. Liu, "Elastic constants of binary Mg compounds from first-principles calculations," *Intermetallics*, vol. 17, pp. 313–318, 2009.

[183] S. Ganeshan, S. Shang, Y. Wang, and Z. -K. Liu, "Temperature dependent elastic coefficients of Mg_2X (X = Si, Ge, Sn, Pb) compounds from first-principles calculations," *J. Alloys Compounds*, vol. 498, no. 2, pp. 191–198, 2010. doi: 10.1016/j.jallcom.2010.03.153.

[184] Y. Liu, W. -C. Hu, D. -J. Li, X. -Q. Zeng, and C. -S. Xu, "Predictions of the structural, electronic, and thermodynamic properties of the anti-fluorite-type Mg_2Sn under pressure from first-principles," *Phys. Scr.*, vol. 88, 2013, Art. no. 045302.

[185] J. De Boor, U. Saparamadu, J. Mao, K. Dahal, E. Müller and Z. Ren, "Thermoelectric performance of Li-doped, p-type $Mg_2(Ge,Sn)$ and comparison with $Mg_2(Si,Sn)$," *Acta Mater.*, vol. 120, pp. 273–280, 2016. doi: 10.1016/j.actamat.2016.08.057.

[186] M. L. Ali, M. Khan, M. A. Al Asad, and M. Z. Rahaman, "Highly efficient and stable lead-free cesium copper halide perovskites for optoelectronic applications: A DFT-based study," *Heliyon*, vol. 9, no. 8, Jul. 29, 2023, Art. no. e18816. doi: 10.1016/j.heliyon.2023.e18816.

[187] B. Wang, Y. Liu, Y. Liu, and J. -W. Ye, "Mechanical properties and electronic structure of TiC, $Ti_{0.75}W_{0.25}C$, $Ti_{0.75}W_{0.25}C_{0.75}N_{0.25}$, $TiC_{0.75}N_{0.25}$ and TiN," *Physica B: Condensed Matt.*, vol. 407, pp. 2542–2548, 2012. doi: 10.1016/j.physb.2012.03.064.

[188] M. Shah, M. Nuruzzaman, A. Hossain, M. Jubair, and M. Zilani, "A DFT insight into structural, mechanical, elasto-acoustic, and anisotropic properties of $Ae PdH_3$ (Ae = Ca, Sr, Ba) perovskites under pressure," *Comput. Condens. Matter*, vol. 34, no. 4, 2023, Art. no. e00774. doi: 10.1016/j.cocom.2022.e00774.

[189] C. M. Kube and M. De Jong, "Elastic constants of polycrystals with generally anisotropic crystals," *J. Appl. Phys.*, vol. 120, no. 16, 2016, Art. no. 165105. doi: 10.1063/1.4965867.

[190] R. Ebrahimi-Jaberi and S. Jalali-Asadabadi, "Anisotropic mechanical behavior and thermal attributes of antiferromagnetic UX_2 (X = P, As, Sb) materials: A density functional and elasticity theories study," *Mater. Chem. Phys.*, vol. 312, no. 1, 2024, Art. no. 128590. doi: 10.1016/j.matchemphys.2023.128590.

[191] M. Payan, M. Khoshini, and R. Jamshidi Chenari, "Elastic dynamic Young's modulus and Poisson's ratio of sand-silt mixtures," *J. Mater. Civil Eng.*, vol. 32, no. 1, 2020, Art. no. 04019314. doi: 10.1061/(ASCE)MT.1943-5533.0002991.

[192] C. Xue *et al.*, "Tailoring Young's modulus by controlling Al bond length and strength using positive Li and negative Mg," *J. Mater. Res. Technol.*, vol. 29, pp. 4682–4696, Mar.–Apr. 2024.

[193] O. K. Orhan and M. Ponga, "Engineering ultra-strong Mg-Li-Al-based lightweight alloys from first principles," 2022, *arXiv:2211.14413*.

[194] C. Zhang, N. Wei, E. Gao, and Q. Sun, "Poisson's ratio of two-dimensional hexagonal crystals: A mechanics model study," *Extreme Mech. Lett.*, vol. 38, 2020, Art. no. 100748. doi: 10.1016/j.eml.2020.100748.

[195] J. Gao, H. Li, X. Sun, X. Zhang, and M. Zhan, "Electro-thermal-mechanical coupled crystal plasticity modeling of Ni-based superalloy during electrically assisted deformation," *Int. J. Plast.*, vol. 157, 2022, Art. no. 103397.

[196] H. Li, C. Shao, D. F. Rojas, M. Ponga, and J. D. Hogan, "Micro-hardness and strain-rate-dependent compressive response of an ultra-lightweight Mg-Li-Al alloy," *J. Alloys Compounds*, vol. 890, 2022, Art. no. 161703.

[197] P. Dryburgh *et al.*, "Determining the crystallographic orientation of hexagonal crystal structure materials with surface acoustic wave velocity measurements," *Ultrasonics*, vol. 108, 2020, Art. no. 106171. doi: 10.1016/j.ultras.2020.106171.

[198] J. Yu, Y. Zhang, Q. Guo, H. Hou, Y. Ma and Y. Zhao, "Effect of pressure on anisotropy in elasticity, sound velocity, and thermal conductivity of vanadium borides," *Adv. Composit. Hybrid Mater.*, vol. 5, no. 3, pp. 2297–2305, 2022. doi: 10.1007/s42114-021-00403-0.

[199] K. Trachenko, B. Monserrat, C. J. Pickard, and V. Brazhkin, "Speed of sound from fundamental physical constants," *Sci. Adv.*, vol. 6, no. 41, 2020, Art. no. eabc8662. doi: 10.1126/sciadv.abc8662.

[200] J. Fu, Z. Wang, W. Liu, J. Yuan, C. Jia and L. Yang, "Effects of heat input on microstructures and mechanical properties of LAZ931 magnesium-lithium alloy by CO_2 laser welding," *Mater. Today Commun.*, vol. 35, no. 1–2, 2023, Art. no. 105536. doi: 10.1016/j.mtcomm.2023.105536.

[201] S. Fan *et al.*, "Elastic anisotropy, thermal conductivity, and tensile properties of MAX phase V_2GaC, Nb_2GaC, and Ta_2GaC: First-principles calculations," *Vacuum*, vol. 209, 2023, Art. no. 111800.

[202] A. Malikov, I. Vitoshkin, A. Filippov, E. Karpov, and K. Kuper, "Effect of post-weld heat treatment on the microstructure, phase composition, and mechanical properties of dissimilar Al-Mg-Li/Al-Cu-Li laser welded joints," *Opt. Laser Technol.*, vol. 173, 2024, Art. no. 110534. doi: 10.1016/j.optlastec.2023.110534.

[203] D. Li and J. Szpunar, "Determination of single crystals' elastic constants from the measurement of ultrasonic velocity in the polycrystalline material," *Acta Metallurgica et Materialia*, vol. 40, no. 12, pp. 3277–3283, 1992. doi: 10.1016/0956-7151(92)90041-C.

[204] S. Daoud, "Mechanical and piezoelectric properties, sound velocity, and Debye temperature of thallium-phosphide under pressure," *Physics, Mater. Sci.*, vol. 1, pp. 1–11, 2014.

[205] Y. Guo and W. Wang, "Effect of doping Zn atom on the structural stability, mechanical, and thermodynamic properties of AlLi phase in Mg-Li alloys from first-principles calculations," *Philos. Mag.*, vol. 100, no. 14, pp. 1849–1867, 2020. doi: 10.1080/14786435.2020.1742397.

[206] M. Wang *et al.*, "First-principles study of the mechanical, electronic, and thermodynamic properties of Mg-Al-Mn ternary compounds," *Vacuum*, vol. 213, no. 5, 2023, Art. no. 112140. doi: 10.1016/j.vacuum.2023.112140.

[207] S. Basri, M. E. Zulkifli, N. S. Hazri, and S. K. Kamarudin, "Quantum behaviour of Mg and Mg-Al-Zn microstructure," *Crystals*, vol. 13, no. 3, 2023, Art. no. 501. doi: 10.3390/cryst13030501.

[208] H. -M. Liu, X. -J. Zhao, Y. -Q. Zhu, and H. Yan, "DFT study on MgAl-layered double hydroxides with different interlayer anions: Structure, anion exchange, host–guest interaction, and basic sites," *Phys. Chem. Chem. Phys.*, vol. 22, pp. 2521–2529, 2020.

[209] Y. Lai *et al.*, "Ion-migration mechanism: An overall understanding of anionic redox activity in metal oxide cathodes of Li/Na-ion batteries," *Adv. Mater.*, vol. 34, 2022, Art. no. 2206039.

[210] H. H. Osman and S. Bobev, "Synthesis, structural characterization, and chemical bonding of $Sr_7Li_6Sn_{12}$ and its quaternary derivatives with Eu and alkaline earth metal (Mg, Ca, Ba) substitutions: A tale of seven Li-containing stannides and two complex crystal structures," *Eur. J. Inorg. Chem.*, vol. 2020, no. 20, pp. 1979–1988, 2020. doi: 10.1002/ejic.202000179.

[211] J. Wang *et al.*, "Effect of Li content on electromagnetic shielding effectiveness in binary Mg-Li alloys: A combined experimental and first-principles study," *J. Mater. Sci.: Mater. Electron.*, vol. 33, no. 7, pp. 3891–3900, 2022. doi: 10.1007/s10854-021-07580-0.

[212] Y. Li, X. Pei, H. Zhang, and M. Yuan, "A first-principle study of interactions between magnesium and metal-atom-doped graphene," *Nanomaterials 2022*, vol. 12, no. 5, 2022, Art. no. 834. doi: 10.3390/nano12050834.

[213] J. Gu, F. Duan, S. Liu, W. Cha, and J. Lu, "Phase engineering of nanostructural metallic materials: Classification, structures, and applications," *Chem. Rev.*, vol. 124, no. 3, pp. 1247–1287, 2024. doi: 10.1021/acs.chemrev.3c00514.

[214] N. C. Rosero-Navarro, R. Kajiura, R. Jalem, Y. Tateyama, A. Miura and K. Tadanaga, "Significant reduction in the interfacial resistance of garnet-type solid electrolyte and lithium metal by a thick

amorphous lithium silicate layer," *ACS Appl. Energy Mater*. vol. 3, no. 6, pp. 5533–5541, 2020. doi: 10.1021/acsaem.0c00511.
[215] Q. Li *et al.*, "In situ observation of the structure of crystallizing magnesium sulfate heptahydrate solutions with terahertz transmission spectroscopy," *Crystal Growth Des.*, vol. 22, pp. 3961–3972, 2022.
[216] P. Nath *et al.*, "High-throughput prediction of finite-temperature properties using the quasi-harmonic approximation," *Comput. Mater. Sci.*, vol. 125, no. 1, pp. 82–91, 2016. doi: 10.1016/j.commatsci.2016.07.043.
[217] P. Jha, "Phonon spectra and vibrational mode instability of $MgCNi_3$," *Phys. Rev. B*, vol. 72, 2005, Art. no. 214502.
[218] E. Braaten and A. Nieto, "Free energy of QCD at high temperature," 1996, *arXiv:hep-ph/9510408*.
[219] F. Ledrappier and L. -S. Young, "Entropy formula for random transformations," *Probabil. Theor. Relat. Fields*, vol. 80, pp. 217–240, 1988.
[220] D. C. Ginnings and G. T. J. J. O. A. C. S. Furukawa, "Heat capacity standards for the range 14 to 1200° K," *J. Am. Chem. Soc.*, vol. 75, no. 3, pp. 522–527, 1953. doi: 10.1021/ja01099a004.
[221] E. Hadjittofis, M. A. Isbell, V. Karde, S. Varghese, C. Ghoroi and J. Heng, "Influences of crystal anisotropy in pharmaceutical process development," *Pharm. Res.*, vol. 35, no. 5, pp. 1–22, 2018. doi: 10.1007/s11095-018-2374-9.
[222] X. Wang *et al.*, "Mechanical and corrosion properties of biodegradable magnesium mini-tubes with different grain morphologies: Size and distribution," *J. Mater. Sci. Technol.*, vol. 183, pp. 165–174, 2024. doi: 10.1016/j.jmst.2023.10.013.
[223] X. Peng, W. -C. Liu, and G. -H. Wu, "Strengthening-toughening methods and mechanisms of Mg-Li alloy: A review," *Rare Metals*, vol. 41, pp. 1176–1188, 2022.
[224] X. Li *et al.*, "The hot deformation behavior, microstructure evolution, and texture types of as-cast Mg-Li alloy," *J. Alloys Compounds*, vol. 831, 2020, Art. no. 154868.
[225] B. -L. Wu, B. Chen, C. -W. Wang, J. -Y. Jiao, Q. -C. Shen and T. -T. J. R. M. Zhou, "Corrosion behavior of a novel Mg-13Li–X alloy with different grain sizes by rapid solidification rate," *Rare Met.*, vol. 41, no. 9, pp. 3197–3204, 2022. doi: 10.1007/s12598-015-0601-7.
[226] J. Grilo, H. Puga, and J. Fernandes, "Influence of melt treatment of AZ91D alloy on phase morphology and corrosion behaviour in Hank's solution," *Corros. Eng., Sci. Technol.*, vol. 56, pp. 504–512, 2021.
[227] Z. Ma *et al.*, "Improvement of microstructure, mechanical property, and corrosion resistance of Mg-9Li–3Al-1Ca alloy through centrifugal casting," *Met. Mater. Int.*, vol. 27, no. 11, pp. 4498–4509, 2021. doi: 10.1007/s12540-020-00690-0.
[228] G. Liu *et al.*, "Microstructure, tensile properties, and corrosion behavior of friction stir processed Mg-9Li-1Zn alloy," *J. Mater. Process. Technol.*, vol. 267, pp. 393–402, 2019.
[229] F. Cao, C. Sun, H. Shang, C. Xiang, and R. Liu, "Microstructure evolution and mechanical properties in an ultralight Mg-2.76Li-3Al-2.6Zn-0.39Y alloy," *Mater. Sci. Eng. A.*, vol. 822, 2021, Art. no. 141680. doi: 10.1016/j.msea.2021.141680.
[230] Y. Q. Yu, X. D. Peng, H. Y. Yi, and J. Liu, "Influence of various heat treatment on corrosion resistance of as-extruded Mg-9Li-3Al-2.5Sr alloys," *Mater. Sci. Forum.*, vol. 788, pp. 41–44, 2014. doi: 10.4028/www.scientific.net/MSF.788.41.
[231] Y. Gao, S. S. Joshi, and K. Nagai, "Prediction of residual performance of corroded RC beams from observed surface cracks by 3D RBSM with MPC," *Eng. Struct.*, vol. 311, no. 1, 2024, Art. no. 118186. doi: 10.1016/j.engstruct.2024.118186.
[232] L. -X. Long *et al.*, "Comparison of microstructure, mechanical property, and degradation rate of Mg–1Li–1Ca and Mg–4Li–1Ca alloys," *Bioact. Mater.*, vol. 26, pp. 279–291. doi: 10.1016/j.bioactmat.2023.02.030.
[233] X. An *et al.*, "Hall-Petch relationship and corrosion behavior of cold-rolled CoNiFe medium entropy alloy," *J. Alloys Compounds*, vol. 807, 2019, Art. no. 151698. doi: 10.1016/j.jallcom.2019.151698.
[234] C. -H. Shih, C. -Y. Huang, T. -H. Hsiao, and C. Lin, "The effect of the secondary phases on the corrosion of AZ31B and WE43-T5 Mg alloys," *Corros. Sci.*, vol. 211, 2023, Art. no. 110920. doi: 10.1016/j.corsci.2022.110920.

[235] Y. -J. Lin and C. Lin, "Galvanic corrosion behavior of friction stir welded AZ31B magnesium alloy and 6N01 aluminum alloy dissimilar joints," *Corros. Sci.*, vol. 180, 2021, Art. no. 109203.
[236] J. Wang *et al.*, "Effects of RE (RE = Sc, Y and Nd) concentration on galvanic corrosion of Mg-Al alloy: A theoretical insight from work function and surface energy," *J. Mater. Res. Technol.*, vol. 24, pp. 6958–6967, 2023. doi: 10.1016/j.jmrt.2023.04.208.
[237] B. Ma, C. Tan, L. Ouyang, H. Shao, N. Wang and M. Zhu, "Microstructure and discharge performance of Mg-La alloys as the anodes for primary magnesium-air batteries," *J. Alloys Compounds*, vol. 918, 2022, Art. no. 165803. doi: 10.1016/j.jallcom.2022.165803.
[238] F. Kozina, "Solidification and characterization of aluminum-magnesium-lithium alloy", University of Zagreb, Croatia, 2024.
[239] W. Song *et al.*, "Microstructure and mechanical properties of as-cast ultralight and high-strength Mg-10Li-3Al-3Zn-xY alloy with multi-precipitates," *Mater. Charact.*, vol. 189, 2022, Art. no. 111972.
[240] J. Li *et al.*, "Microstructure and corrosion behavior of as-extruded Mg-6.5Li-xY-yZn alloys," *J. Alloys Compounds*, vol. 823, no. 11, 2020, Art. no. 153839. doi: 10.1016/j.jallcom.2020.153839.
[241] H. Feng, S. Liu, Y. Du, T. Lei, R. Zeng and T. Yuan, "Effect of the second phases on corrosion behavior of the Mg-Al-Zn alloys," *J. Alloys Compounds*, vol. 695, no. 5, pp. 2330–2338, 2017. doi: 10.1016/j.jallcom.2016.11.100.
[242] H. Chen, K. Zhang, C. Yao, J. Dong, Z. Li and C. Emmelmann, "Effect of Al_2Gd on microstructure and properties of laser clad Mg–Al–Gd coatings," *Appl. Surf. Sci.*, vol. 330, pp. 393–404, 2015. doi: 10.1016/j.apsusc.2014.11.132.
[243] Z. Han, W. Xu, C. -B. Liu, L. -Y. Cui, and R. -C. Zeng, "Superior discharge performance of Mg-air battery: The influence of anodic intermetallic compounds $Mg_{41}Nd_5$ in Mg-4Li-3Nd-0.2Zn alloy," *J. Mater. Res. Technol.*, vol. 25, no. 3, pp. 7024–7038, 2023. doi: 10.1016/j.jmrt.2023.07.122.
[244] L. Zhu *et al.*, "Tailoring the formability and planar anisotropy of Al-Mg-Si-Cu-Zn alloys via cross hot rolling and two-stage cold rolling," *J. Alloys Compounds*, vol. 985, no. 11, 2024, Art. no. 174089. doi: 10.1016/j.jallcom.2024.174089.
[245] R. -C. Zeng, W. -C. Qi, Y. -W. Song, Q. -K. He, H. -Z. Cui and E. -H. Han, "*In vitro* degradation of MAO/PLA coating on Mg-1.21Li-1.12Ca-1.0Y alloy," *Front. Mater. Sci.*, vol. 8, no. 4, pp. 343–353, 2014. doi: 10.1007/s11706-014-0264-6.
[246] M. Samiee, M. Hanachi, Z. Seyedraoufi, M. Eshraghi, and Y. Shajari, "Biodegradable magnesium alloy coated with TiO_2/MgO two-layer composite via magnetic sputtering for orthopedic applications: A study on the surface characterization, corrosion, and biocompatibility," *Ceram. Int.*, vol. 47, pp. 6179–6186, 2021. doi: 10.1016/j.ceramint.2020.10.196.
[247] M. M. Sabzehmeidani and M. Kazemzad, "Recent advances in surface-mounted metal–organic framework thin film coatings for biomaterials and medical applications: A review," *Biomater. Res.*, vol. 27, no. 1, 2023, Art. no. 115. doi: 10.1186/s40824-023-00454-y.
[248] S. -M. Hung, H. Lin, H. -W. Chen, S. -Y. Chen, and C. -S. Lin, "Corrosion resistance and electrical contact resistance of a thin permanganate conversion coating on dual-phase LZ91 Mg-Li alloy," *J. Mater. Res. Technol.*, vol. 11, pp. 1953–1968, 2021. doi: 10.1016/J.JMRT.2021.02.050.
[249] J. Li, L. Jin, S. Yi, X. Zhang, J. Dong and M. Luo, "Deformation mechanisms of β-Li in Mg-Li dual-phase alloy and effects of surface oxide layer," *Mater. Sci. Eng. A*, vol. 889, 2024, Art. no. 145856.
[250] Y. Ma *et al.*, "Effect of air-formed film on corrosion behavior of magnesium-lithium alloys," *J. Magnes. Alloys*, vol. 11, no. 11, pp. 4325–4337, Nov. 2022. doi: 10.1016/j.jma.2022.11.
[251] N. Singh, U. Batra, K. Kumar, N. Ahuja, and A. Mahapatro, "Progress in bioactive surface coatings on biodegradable Mg alloys: A critical review towards clinical translation," *Bioact. Mater.*, vol. 19, no. 8, pp. 717–757, 2023. doi: 10.1016/j.bioactmat.2022.05.009.
[252] M. C. Rossi, R. F. dos Santos, P. A. B. Kuroda, and C. Afonso, "Characteristics of ceramic-like coatings obtained by plasma electrolyte oxidation on different Ti alloys," *Boletín de la Sociedad Española de Cerámica y Vidrio*, vol. 63, pp. 33–46, 2024. doi: 10.1016/j.bsecv.2023.04.002.

[253] J. Zhao, J. Zhang, W. Liu, G. Wu, and L. Zhang, "Effect of Y content on microstructure and mechanical properties of as-cast Mg–8Li–3Al–2Zn alloy with duplex structure," *Mater. Sci. Eng. A*, vol. 650, pp. 240–247, 2016. doi: 10.1016/j.msea.2015.10.067.

[254] A. Huntz, J. Zhao, A. Boumaza, and G. Moulin, "Parameters affecting oxide adherence in nickel-based alloys and techniques allowing estimation of adherence," *Mater. Sci. Technol.*, vol. 4, no. 5, pp. 470–478, 1988. doi: 10.1179/mst.1988.4.5.470.

[255] S. Murarka and T. F. Retajczyk, "Effect of phosphorus doping on stress in silicon and polycrystalline silicon," *J. Appl. Phys.*, vol. 54, no. 4, pp. 2069–2072, 1983. doi: 10.1063/1.332255.

[256] P. Xiang, J. -W. Sun, H. -J. Liu, G. -H. Wu, and W. Liu, "Microstructure and corrosion behavior of as-homogenized and as-extruded Mg−xLi−3Al−2Zn−0.5Y alloys ($x = 4$, 8, 12)," *Trans. Nonferrous Met. Soc. China*, vol. 32, no. 1, pp. 134–146, 2022. doi: 10.1016/S1003-6326(21)65783-7.

[257] X. Lu *et al.*, "A systematic review and network meta-analysis of biomedical Mg alloy and surface coatings in orthopedic application," *Bioinorg. Chem. Appl.*, vol. 2022, no. 1, 2022. doi: 10.1155/2022/4529520.